Journal of Controlled Release 311–312 (2019) 147–161

Contents lists available at ScienceDirect

Journal of Controlled Release

journal homepage: www.elsevier.com/locate/jconrel

NIR- and thermo-responsive semi-interpenetrated polypyrrole nanogels for imaging guided combinational photothermal and chemotherapy

Loryn E. Theune[a], Jens Buchmann[b], Stefanie Wedepohl[a], Maria Molina[a], Jan Laufer[b], Marcelo Calderón[a,c,d,*]

[a] Freie Universität Berlin, Institute of Chemistry and Biochemistry, Takustr. 3, 14195 Berlin, Germany
[b] Institut für Physik, Martin-Luther-Universität Halle-Wittenberg, Von-Danckelmann-Platz 3, 06120 Halle (Saale), Germany
[c] POLYMAT and Applied Chemistry Department, Faculty of Chemistry, University of the Basque Country UPV/EHU, Paseo Manuel de Lardizabal 3, 20018 Donostia-San Sebastián, Spain
[d] IKERBASQUE, Basque Foundation for Science, 48013 Bilbao, Spain

A B S T R A C T

Versatile, multifunctional nanomaterials for theranostic approaches in cancer treatment are highly on demand in order to increase therapeutic outcomes. Here, we developed thermo-responsive nanogels equipped with the efficient near-infrared (NIR) transducing polymer polypyrrole (PPY) for combinational photothermal and chemotherapeutic therapy along with photoacoustic imaging ability. Long-term stability and water-dispersibility of PPY was achieved using semi-interpenetration method for *in situ* polymerization of PPY into hydrophilic thermo-responsive nanogels. The semi-interpenetrated nanogels of spherical shape and with hydrodynamic sizes of around 200 nm retained the temperature response behaviour and exhibit excellent photothermal transducing abilities in the NIR region. The PPY nanogels served as photoacoustic contrast agents, which allowed determination of biodistribution profiles *ex vivo*. In addition, we developed a new method for biodistribution determination based on the photothermal response of the nanogels with an accuracy down to 12.5 μg/mL. We examined the ability of the nanogels as photothermal agents and drug delivery systems *in vitro* and *in vivo*. We showed that they efficiently inhibit tumor growth with combinational effects of chemotherapeutics and photothermal treatment. Our work encourages further exploration of nanogels as functional stabilizing matrix for photothermal transducers and their application as drug delivery devices in combination with photothermal therapy and imaging.

1. Introduction

Photothermal transducing agents able to transform light into heat gained increased interest for the application in photothermal therapy (PTT) of cancer [1–3]. In particular, particles able to transform near-infrared (NIR) light between 700-950 nm attracted increased attention since biological tissue shows particularly low absorbance and scattering of light within this range. As a result, the penetration depth of NIR light into tissue is significantly greater than light of other wavelengths, *e.g.* light of the UV–visible range, and can reach up to several centimetres deep. Taking advantage of this deep penetration, materials able to transduce NIR light to heat offer minimally invasive approaches for cancer treatment. With the use of external laser irradiation they deliver high thermal energy to the cancerous tissue, allow adjustable energy dosing, and precise local control rendering them into efficient agents for thermal ablation of tumors and yet minimizing harm to surrounding healthy tissue [1–3].

Besides inorganic nanoparticles [4–7] and carbon based NIR transducers [8–10], semi-conducting polymers like polypyrrole (PPY) [11–13], polyaniline (PANI) [14–17], and poly(3,4-ethylenedioxythiophene) polystyrene sulphate (PEDOT:PSS) [18,19] emerged as excellent materials for PTT of cancer with high photostability and good biocompatibilities. In particular, PPY based materials were demonstrated to be suitable materials for biomedical applications like biosensors [20,21], biomaterials in tissue engineering [22], and neural prosthetics [23,24] and thus gained increased interest for PTT [25,26]. First reports of nano-sized PPY particles in PTT of cancer indicate promising results *in vitro* and *in vivo* by thermal ablation of tumor cells upon exposure to NIR light [11,12,27,28].

The photothermal effect of PPY based materials additionally allow their use as a contrast agent in photoacoustic (PA) imaging enabling particle localization. PA imaging is an emerging non-invasive technique that provides 3D images of absorption-based contrast with high spatial resolution and allows a comparative and quantitative image intensity analysis [1]. PA imaging typically uses short (nanoseconds) optical excitation pulses to induce local thermal expansion of the tissue which translates into acoustic waves. The spatial distribution of the optical absorption, and hence the local abundance of chromophores, is encoded

* Corresponding author at: POLYMAT and Applied Chemistry Department, Faculty of Chemistry, University of the Basque Country UPV/EHU, Paseo Manuel de Lardizabal 3, 20018 Donostia-San Sebastián, Spain.
E-mail address: marcelo.calderon@polymat.eu (M. Calderón).

https://doi.org/10.1016/j.jconrel.2019.08.035
Received 24 June 2019; Received in revised form 25 August 2019; Accepted 29 August 2019
Available online 30 August 2019

onto the time-course of the waves, which are detected outside the organism or sample. From these data sets, three-dimensional images are reconstructed that show the spatial distribution of the absorbing chromophores within the illuminated volume. As a result, light-to-heat transducing materials increase the PA signal intensity translating these materials into intrinsic theranostic devices enabling imaging guided therapy approaches. For pure PPY nanoparticles the suitability as PA contrast agent was demonstrated by Dai and coworkers who showed the ability to visualize the particles down to a depth of 4 cm in muscle tissue upon exposure to laser light of 808 nm [29]. In the same group, PPY particles were successfully equipped with a gadolinium chelate which was used to confirm the good correlation between PA and magnetic resonance imaging [30].

Intrinsic imaging modalities additionally are advantageous for the determination of biodistribution profiles of new materials, which is a key parameter for the evaluation of new drug delivery agents. With a label-free detection of the particles, one can disclaim additional synthetic modifications which could alter occurring biological interactions after administration.

As PPY in its pure form is water insoluble, particle stabilization is crucial for a use in biomedical applications. In first reports for PPY nanoparticles for PTT applications, stabilization was achieved by wrapping the final particles using the polymers polyvinyl pyrrolidone (PVP) or polyvinyl alcohol (PVA) added during the polymerization process [11,12]. With promising results of initial work in combinational treatments using PTT along with other therapies like chemotherapy and radiotherapy [31–34], it stands to reason that a rational design of the stabilizing matrix *e.g.* equipping them with stimuli responsive materials can implement new functionalities for the use of the particles in combinational therapy approaches [3].

One possible option is the incorporation of PPY into hydrophilic nanogels, which are three-dimensional cross-linked polymeric particles that emerged as a versatile tool for the encapsulation of guest molecules [35,36]. In particular upon usage of 'smart' polymers for their synthesis, nanogels which change their physico-chemical properties in response to internal or external stimuli can serve as effective drug delivery systems with controlled cargo release upon application of a trigger [35,37–40]. For example, we recently developed thermo-responsive nanogels based on the temperature-responsive polymers *poly*-(N-isopropyl acrylamide) (PNIPAM) and *poly*-(N-isopropyl methacrylamide) (PNIPMAM) which shrink upon application of a temperature trigger and release encapsulated proteins along with the expulsion of water [41,42]. As crosslinker for these nanogels, we used biocompatible dendritic polyglycerol (dPG), which stabilized the nanogels and decreased protein surface adhesion, both important factors for the biodistribution of nanocarriers [43–47].

In a preliminary work we could recently show the feasibility of thermo-responsive nanogels as a stabilizing matrix for the photothermal transducing polymer PANI and we could demonstrate the applicability of the resulting nanogels as PTT agent [16]. For the introduction of PANI we used semi-interpenetration method. Semi-interpenetration is defined as the physical entanglement of a linear polymer in a cross-linked polymeric network and is typically achieved through the formation of one system in presence of the other [48,49]. It emerged as an elegant tool for the inclusion of new capabilities to nanogels through the penetration with functional polymers. The great advantage of the semi-interpenetration method is that the individual properties of both the nanogels and the interpenetrating polymer are retained by their non-covalent linkage. For a potential use of the semi-interpenetrated materials as drug delivery agent, a proper understanding of the interpenetrating process and resulting structure, *e.g.* the localization of the interpenetrating polymer within the nanogels is important. In the case of stimuli-responsive nanogels, additionally a thorough understanding of structural changes influencing the particles properties under exposure to the stimulus is relevant to determine suitable candidates for an application *in vivo*.

In the present study, we fabricate thermo-responsive nanogels loaded with the photothermal transducing polymer PPY for combinational photothermal- and chemotherapy along with PA imaging modalities. We prepared thermo-responsive nanogels with different volume phase transition temperatures (VPTTs) by precipitation polymerization using acrylated dPG as cross-linker for PNIPAM, PNIPMAM or copolymers of both and investigated their suitability for a semi-interpenetration with PPY [41]. The photothermal transducing property of PPY endows the nanogels with a dual-response for temperature and NIR light. The generated heat under exposure to NIR can thereby be used as the trigger for the thermo-responsive network as well as for photothermal ablation of cancer. Additionally, the suitability of the prepared nanogels for PA contrast enhancement was assessed using mouse organs as a model. Based on that we developed a new label free method for the establishment of biodistribution profiles using the photothermal response of the particles. Finally, the nanogels are evaluated *in vitro* and *in vivo* as drug delivery agent and in combination with photothermal induced ablation of tumor cells. The promising therapeutic outcome encourages further exploration of multifunctional polymer based nanoplatforms for combinational therapy approaches against cancer.

2. Materials and methods

2.1. Materials

The following materials were used as purchased: Acryloyl chloride (Ac-Cl, Aldrich, 97%), triethylamine (TEA, Acros, 99%), dry *N*,*N*-dimethylformamide (DMF, Acros, 99.8%), sodium dodecyl sulphate (SDS, Sigma, ≥98%), potassium persulfate (KPS, Merck, ≥99%), pyrrole (Sigma, 98%), ammonium persulfate (APS, Sigma, ≥98%). N-isopropylacrylamide (NIPAM, Sigma, 99%) and N-Isopropylmethacrylamide (NIPMAM, Sigma, 97%) were recrystallized in n-hexane prior use.

2.2. Methods

The synthesis of thermoresponsive nanogels based on PNIPAM, PNIPMAM and 1:1-copolymer (Co) of both was done as reported using acrylated dPG as macromolecular crosslinker [41]. In brief, 70 mg monomers, 30 mg acrylated dPG (synthesis see SI) and SDS (1.8 mg) were dissolved in 4 mL distilled water. The reaction mixture was purged with argon for at least 15 min before transferring it to a hot bath at 70 °C. After 5 min, an aqueous solution of KPS (3.3 mg, 1 mL) was added quickly to initiate the polymerization. The mixture was left stirring at 70 °C for 3 h, followed by purification *via* dialysis (regenerated cellulose, molecular weight cut-off (MWCO) of 50 kDa) in water. After lyophilisation, the product was obtained as a white cotton-like solid. Yield 80–90%. ^{1}H NMR spectra of the resulting nanogels see SI.

2.2.1. Semi-Interpenetration of thermoresponsive nanogels with PPY

Dry nanogels were swollen in a solution of pyrrole·HCl with a nanogel concentration of 10 mg/mL. After complete dissolution the polymerization process was initiated by quickly adding an APS solution (same molarity than pyrrole·HCl, half the volume of swelling solution). After 30 min, polymerization was finished and the semi-interpenetrated PPY nanogels were transferred into a dialysis bag (regenerated cellulose, MWCO 50 kDa, Carl Roth) and dialysed in deionized water for at least 3 days. The nanogels were stored in solution, concentrations were adjusted by dialysis against concentrated polyethylene glycol (100 kDa) solution.

The nanogels particle sizes given as hydrodynamic diameter, dispersity, and VPTT were measured at various temperatures by dynamic light scattering (DLS) using Malvern Zetasizer Nano-ZS 90 (Malvern Instruments) equipped with a red He Ne laser (λ = 633 nm, 4.0 mW) or a green DPSS laser (λ = 532 nm, 50.0 mW) under a scattering angle of

173°. All samples were maintained for stabilization at the desired temperature for 2–5 min before testing. Particle sizes and size distributions (PDI) are given as the average of 3 measurements from the intensity distribution curves. For determination of the VPTT, the sizes of the nanogels measured in a temperature range of 25–55 °C (step size 0.5 °C) was plotted against the temperature. The VPTT is defined as the temperature at the inflection point of the normalized size curve.

The swelling degree of nanogels is defined by the ratio between particle volume in swollen state (25 °C) and collapsed state (55 °C).

The effect of NIR irradiation on size of the nanogels was assayed by irradiating a 0.25 mg/mL or 0.1 mg/mL nanogel solution for 3 min with an infrared diode laser module (FC-D-785 CNI, λ = 785 nm, 500 mW) and immediately measuring their size by DLS.

The polymerization process of PPY was followed by time dependent UV-VIS absorbance measurements on a Scinco S-3100 spectrometer or in 96-well plates using a Tecan Infinite M200Pro microplate reader.

Nanogels shape and size in dry state was investigated by transmission electron microscopy (TEM). Samples were prepared on carbon-coated copper grids (300 mesh, Quantifoil) and the nanogels were visualized using the TEM mode of the Hitachi Scanning Electron Microscope (SU8030) (20 kV).

2.2.2. Photothermal effect

The heat production of the nanogels was measured at different concentrations placing a 20 µL sample in a transparent eppendorf tube and irradiating with an infrared diode laser module (FC-D-785 CNI, λ = 785 nm, 500 mW) or NIR lamp (hydrosun 750, Hydrosun Medizintechnik GmbH) equipped with water filter and additional band pass filter (721 nm −1000 nm, $T > 70\%$, FGL9, ThorLabs). During 5 min of irradiation, the temperature increase was monitored with an infrared camera (FLIR E30, 25° Optic, 60 Hz).

2.2.3. Encapsulation and release studies

The encapsulation efficiency of the thermoresponsive nanogels and semi-interpenetrated nanogels was evaluated for the anti-cancer drug Methotrexate (MTX). Therefore, MTX (Sigma, ≥98%) was solubilized in water by adding NaOH (1 M) to an aqueous MTX dispersion until full solubility was reached. Afterwards the pH of this solution was adjusted to neutral pH values by dropwise addition of HCl (1 M). The resulting MTX stock solution was stable up to several months and was stored in the fridge.

For nanogels which could be redissolved after drying (non-interpenetrated and PPY/PNIPMAM-dPG), the encapsulation was achieved by swelling the dry nanogels in an aqueous solution of MTX (1 mg MTX/mg NG, c = 5 mg/mL). For all other nanogels, a nanogel solution was heated to 55 °C in a water bath for at least 30 min to collapse the nanogels. Then, a concentrated solution of MTX (1 mg MTX/mg NG, c = 30 mg/mL) was added and the mixture was cooled down in an ice bath to swell the nanogels. All nanogel-MTX solutions were stored in the fridge overnight prior purification by gel filtration (Sephadex G-25 PD-10, GE Healthcare). The amount of separated free MTX was determined by UV-VIS spectroscopy using absorbance at 380 nm. Encapsulation efficiency (EE%) was calculated using the following equation:

$$EE\,[\%] = \frac{m\,(MTX_{init.}) - m\,(MTX_{free})}{m\,(MTX_{init.})} \cdot 100 \quad (1)$$

The release profiles of MTX from the nanogels was determined using dialysis method. The nanogel solution was transferred into a dialysis bag (Float-A-Lyzer G2, MWCO 300 kDa, VWR) with 6 mL of surrounding acceptor medium (PBS pH 7.4). At indicated time points the whole acceptor medium was collected and replaced by fresh buffer solution. The collected fraction was lyophilized, redissolved and MTX content was measured by UV–Vis spectroscopy using absorbance at 380 nm. NIR induced release was assayed applying 5 min of NIR irradiation (785 nm, 500 mW) on indicated time points.

2.2.4. Evaluation of photothermal ablation ability and combinational therapy in vitro

A549 cells (Leibniz Institute DSMZ – German Collection of Microorganisms and Cell Cultures, #ACC 107) were seeded into 96 well plates in DMEM (Thermo Fisher Scientific) with 10% FBS (Merck Millipore) and 1% Penicillin/Streptomycin (Thermo Fisher Scientific) at a density of 10,000 cells/well. Cells were incubated with nanogel solutions with and without loaded MTX for 48 h. The nanogels concentrations of all applied solutions were adjusted according to their absorbance at 785 nm (0.42 mg/mL PPY/PNIPAM-dPG, 1.0 mg/mL PPY/Co-dPG and, 0.67 mg/mL PPY/PNIPMAM-dPG, MTX loaded nanogels as their non-loaded analogues). After incubation, half of the wells containing cells were irradiated for 6 min with an infrared diode laser module (FC-D-785 CNI, λ = 785 nm, 500 mW). After overnight incubation, cell viability was assessed by MTT test. For this, 10 µL/well MTT solution (5 mg/mL in PBS) was added in fresh medium to the cells and incubated for 4 h at 37 °C. Afterwards, the cell culture supernatant was removed and 100 µL/well of isopropanol containing 0.04 M HCl was added. Absorbance was read at 570 nm in a Tecan Infinite M200Pro microplate reader. Relative cell viabilities were calculated by dividing absorbance values of wells with treated cells by the values of untreated cells (100%). Two replicate wells were run for each sample and the experiment was repeated twice.

2.2.5. Tolerability of nanogels in vivo

All animal studies were performed in accordance to national and local guidelines and regulations as described in the approved Tierversuchsantrag G 0030/15 (Landesamt Berlin für Gesundheit) from 20.09.2018 for the EPO GmbH Berlin-Buch. During all studies, behaviour of the mice was monitored regularly as an indicator for the tolerability of the treatments and to ensure the animals do not feel pain or enduring stress.

In the first part of the study, healthy 6–8 weeks old female nude (NMRI, nu/nu) mice were injected with increasing doses (10, 20, 40, 70 or 100 mg/kg) of nanogels into their tail vein and body weight changes were monitored over the course of 2 weeks. In the second part of the study, the maximum tolerated dose found in the first part (100 mg/kg) was injected on five consecutive days and the tolerability was monitored by body weight for two weeks. One, respective 14 days after the last injection, selected organs were collected and fixed in formalin for 24 h.

Hematoxylin and Eosin (H&E) stained slides prepared from formalin-fixed paraffin embedded tissue samples of liver, lung, kidney, spleen and heart of treated and untreated mice were examined by pathologists at EPO GmbH Berlin-Buch.

2.2.6. Biodistribution

Biodistribution profiles of the nanogels were generated *ex vivo* using the photothermal response of the nanogels present in the organs and the results were validated by photoacoustic measurements. For the evaluation of tumor accumulation, 6–8 week old female nude (NMRI, nu/nu) mice bearing A549 lung cancer xenografts (average tumor volume 0.13 cm^3 at day 7 after subcutaneous (s.c.) cell inoculation) were treated once with an intravenous (i.v.) injection of 100 mg/kg of nanogels or PBS *via* tail vein. 2 h, 6 h, 12 h, 24 h, and 48 h after the injections 3 mice per group were sacrificed and organs were sampled and snap-frozen or formalin-fixed.

2.2.7. Photothermal response

Photothermal response of organ samples was measured in two modalities. First, in order to validate and establish the method, formalin fixed full organs were irradiated with a NIR lamp (hydrosun 750, Medizintechnik GmbH) equipped with a water filter and additional band pass filter (721 nm - 1000 nm, $T > 70\%$, FGL9, ThorLabs,

d = 10 cm). The temperature increase within 5 min irradiation was recorded by an IR camera. Second, organs were homogenized (Homogenisator, VDI12, VWR) and diluted in PBS (pH 7.4), and 20 μL samples were irradiated with infrared diode laser module (FC-D-785 CNI, λ = 785 nm, 500 mW). For quantitative analysis, a standard curve was prepared of temperature *vs* concentration values of nanogel solutions irradiated in the same way. The temperature values of irradiated organ samples were corrected by values of irradiated untreated organs and concentrations were obtained from exponential fit of the calibration curve. Values are given as average of three different organs expressed as percent of injected dose (%ID) per organ or per g of organ and calculated using following equations:

$$\%ID = \frac{\frac{c}{DF}\cdot V}{ID}\cdot 100 \quad (2)$$

$$ID = dx\cdot BW \quad (3)$$

where c is defined as particle concentration, DF is the dilution factor, V sample volume after homogenisation, d is the dose per injection, x reflects the number of injections, and BW is the bodyweight at the day of first injection.

2.2.8. Photoacoustic imaging

Tomographic 3D PA images of formalin-fixed organs and snap-frozen tumors were acquired *ex vivo* using a Fabry-Perot-based ultrasound scanner [50,51]. The organs were placed on the scanner and acoustically coupled with PBS. PA signals were generated using excitation pulses of 8 ns duration at two different wavelengths (620 nm and 800 nm) provided by an OPO laser (Innolas Spitlight 1000 OPO). The pulse energies were 8 mJ and 13 mJ, respectively. The samples were illuminated by a Gaussian beam of approximately 20 mm diameter ($1/e^2$).

3D image data sets of organs were acquired over an *x-y* scan area of 16.2 × 16.2 mm^2 with a step size of $dx = dy = 180$ μm. Tumors were measured over a 20.0 × 20.0 mm^2 scan area ($dx = dy = 200$ μm). The time-resolved PA signals comprising the data sets were recorded using 20 MHz detection bandwidth and 15 μs acquisition length. 3D PA images were reconstructed using the time-reversal algorithm of the k-Wave toolbox [52] and the data sets were two-fold upsampled before reconstruction to improve lateral resolution [53]. The intensities of the images were normalized with respect to the pulse energy at the two excitation wavelengths. To allow a quantitative comparison, *x-y* maximum intensity projections (MIPs) of the 3D images were calculated. Regions of interest (ROI) corresponding to the organ shapes were manually segmented using polygons and the average signal intensities of the MIPs and the standard deviations inside the ROIs were calculated.

2.2.9. Anti-tumor efficiency

6–8 weeks old female nu/nu mice were injected s.c. with 1 × 10^7 A549 cells to form xenograft tumors in the flank. Treatments were started when the tumor volume (TV) reached approximately 100 mm^3 which was designated as day = 0 (d0). Mice were homogenously distributed into 11 groups ($n = 6$). The tumor bearing mice were treated intratumorally (i.t.) with injections of 30 μL nanogels solution (10 mg/mL) of PPY/PNIPAM and PPY/Co, purely and loaded with MTX (10 wt %), followed by irradiation of the tumor site with infrared diode laser module (FC-D-785 CNI, λ = 785 nm, 500 mW) for 5 min. The remaining 7 groups including untreated mice (PBS (i.t.)), NIR exposed mice (PBS (i.t.) + laser), MTX treated mice (10 mg/kg every 3 days, intraperitoneal (i.p.)), PPY/PNIPAM and PPY/Co without NIR irradiation, and MTX loaded PYY/PNIPAM and PPY/Co without laser served as controls. Temperature changes at the tumor site were monitored using an IR camera (FLIR E30, 25° Optic, 60 Hz). Tumor sizes were determined with a calliper and was calculated as TV = (LxW^2)/2, where L is tumor length and W is tumor width.

For analysis of mild photothermal treatment i.t. (temperature at the tumor site limited to a maximum of 45 °C) and tumor inhibition after i.v. administration of the nanogels, mice bearing A549 tumors (TV 300 mm^3) were used. Here, the day of laser treatment after last nanogel injection was designated as d0. Tumor bearing mice were treated either i.t. with PPY/Co nanogel solutions (10 mg/mL; 1 mg/TV) or i.v. (100 mg/kg) for 5 consecutive days. For mice treated i.t., NIR irradiation of the tumor site was performed immediately after injection for 5 min, or 15 min respectively ($n = 3$). PBS treated mice (i.t.) served as control. For i.v. treatment with PPY/Co mice were separated in 2 groups (n = 3) and irradiated for 5 min after the 3rd injection of nanogels and after the 5th, or only once after 5th injection.

3. Results and discussion

3.1. Synthesis of photothermal transducing thermo-responsive nanogels

For the generation of dual NIR- and thermo-responsive nanogels suitable for imaging guided combinational photothermal and chemotherapy, we were interested in the use of thermo-responsive nanogels as 'smart' stabilizing matrix for the NIR transducing polymer PPY. To optimize the behaviour of resulting nanogels after systemic administration, particularly the influence of the hydration state of the thermo-responsive network on the biodistribution profile and the tumor accumulation should be evaluated. We therefore aimed to synthesize thermo-responsive nanogels with similar physico-chemical properties but different hydration states at 37 °C body temperature. To achieve this, we chose the thermo-responsive polymers PNIPAM and PNIPMAM for the generation of nanogels. The two polymers have an almost identical structure with the difference of PNIPMAM bearing a methyl group in its polymeric backbone and thus have a higher transition temperature than PNIPAM [41]. To obtain nanogels which are in different hydration states after systemic administration, their VPTTs need to be tuned to values below, respectively above 37 °C body temperature.

We therefore synthesized thermo-responsive nanogels based on PNIPAM and PNIPMAM using macromolecular dPG as cross-linker. We could successfully tune the VPTT of the nanogels dependent on whether we used either only one of the thermo-responsive polymers or performing a copolymerization of both (Table S1). PNIPAM-dPG nanogels exhibited a transition temperature of 34 °C and are thus in their collapse state at 37 °C. In contrast, copolymeric nanogels with a 1:1 wt. ratio of PNIPAM and PNIPMAM (Co-dPG) and PNIPMAM-dPG nanogels have their transition at 40 °C, respectively 47 °C. Thus, both are in a swollen state at 37 °C body temperature. All nanogels had neutral zeta-potential, sizes between 130 and 180 nm and showed similar swelling-shrinking ratios rendering them into feasible candidates for a comparative evaluation of the hydration state influence on the nanogels behaviour.

First, we were interested in the ability of these nanogels to act as stabilizing matrix for PPY. To introduce PPY to the thermo-responsive nanogels we used semi-interpenetration. This was performed by swelling dry nanogels in an acidified solution of pyrrole and initiating its *in situ* polymerization within the nanogels network with APS (Fig. 1). The variation of the molarity of monomer solution revealed no major impact on the final particle size in hydrated state with sizes of all semi-interpenetrated nanogels of around 200 nm (Table 1). However, at higher molarity copolymeric and NIPMAM based PPY nanogels aggregated strongly upon crossing the VPTT of the thermo-responsive network making theses nanogels unsuitable for systemic administration. We found that for nanogels with higher VPTT (equating higher PNIPMAM content) stable nanogels are only obtained when lower molarity of pyrrole is used. A possible reason for this behaviour could be the size difference of the thermo-responsive nanogels with PNIPMAM-dPG nanogels being approximately 60 nm smaller than their PNIPAM analogues. As similar sizes after semi-interpenetration are reached for all nanogels, we hypothesize that a higher ratio of PPY

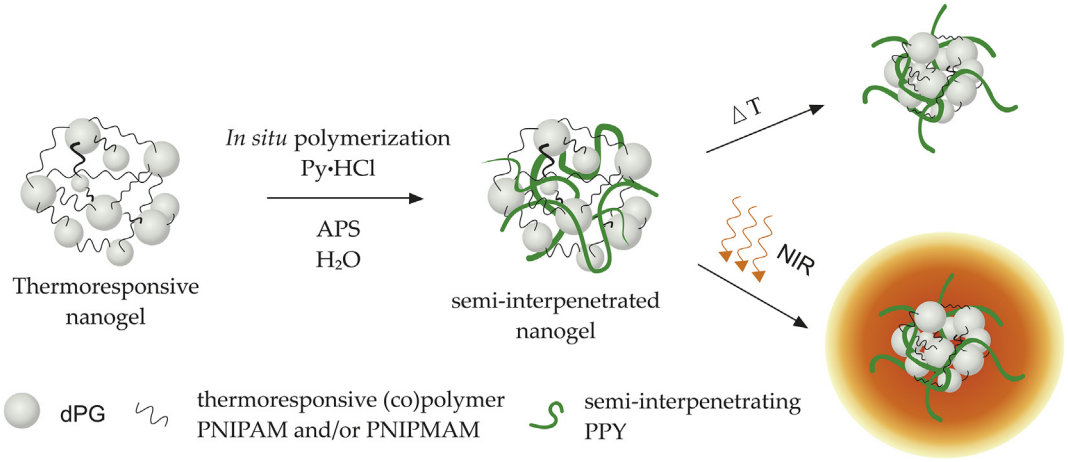

Fig. 1. Synthesis of dual responsive nanogels by semi-interpenetration of PPY into thermo-responsive nanogels. The nanogels change their hydration state and shrink either by application of temperatures above the VPTT of the thermo-responsive network, or due to the locally generated heat by the PPY chains under NIR exposure.

chains will partially be outside or on the surface of the nanogel network in case of copolymeric and PNIPMAM based networks. We suppose that this ratio even will be increased upon crossing the transition temperature of the thermoresponsive network and its resulting contraction (Fig. 1). This assumption is supported by our findings for semi-interpenetration of PNIPAM-dPG nanogels with charged polymers showing a change in the zeta-potential upon crossing the VPTT indicating the exposure of the inner semi-interpenetrating network [54]. Due to the water-insolubility of the PPY, a high ratio of exposed PPY could lead to a loss of the stabilizing ability of the thermoresponsive network. Thus, a high PPY content and smaller size of the thermo-responsive network lead to aggregation of the resulting semi-interpenetrated nanogels at high temperatures.

In order to confirm the entanglement of PPY chains within the nanogels network, we performed the semi-interpenetration in a similar manner but in the macroscale using thermo-responsive hydrogels prepared with the same building blocks as used for the nanogels. In Fig. 2A-E it can be nicely seen that the polymerization of pyrrole starts at the hydrogels surface. With time, the whole solution turns black forming PPY also outside the hydrogel structure. These non-interpenetrated PPY chains precipitated overnight (Fig. 2F) in similar manner to polymerization performed in absence of a hydrogel (Fig. 2 insets a,e,f). Short oligomeric pyrrole chains yielding a greenish colour of the solution can be sufficiently removed by dialysis while non-interpenetrated longer PPY chains precipitate (Fig. 2G). After purification, a stable black hydrogel (Fig. 2H) is obtained underlining the stabilizing ability of the gels network for PPY chains and successful interpenetration. Transferring this to the nanoscale, the absence of PPY precipitates indicate that PPY formation is only happening within the nanogels probably promoted by the greater surface area of the nanogels in comparison to the macroscopic gel and their dispersion in the whole solution. This is in good agreement with findings from Fernández-Barbero and coworkers who could demonstrate uniform distribution of PPY within micro-scale thermo-responsive gels when the penetration reaction was performed at temperatures below the VPTT of the microgels (in the swollen state) [55].

Another aspect which may influence the formation of stable interpenetrated nanogels could be the polymerization kinetic, which we found to be faster for the semi-interpenetration process performed at higher molarity of pyrrole (Fig. 3A). Eventually, when the polymerization is progressing too fast, formed PPY chains are not sufficiently entangled or not located in the inside of the nanogel network, leading to an aggregation upon the shrinkage of the thermo-responsive network.

Absorbance spectra of the reaction mixture clearly show increasing absorbance in the NIR region due to increasing chain length of PPY (Fig. 3B). After purification, the obtained nanogels show the characteristic absorbance spectrum of PPY demonstrating the successful interpenetration (Fig. 3C). As a result of the higher molarity of pyrrole solution used for PNIPAM-dPG nanogels, these nanogels have a higher PPY content than their copolymeric and NIPMAM based analogues. This is evidenced by a stronger absorbance for same nanogel concentration. Besides the stability upon heating, long-term stability of the nanogels over several months was assayed by frequently measuring their hydrodynamic size demonstrating stability of all PPY nanogels up to six months.

As can be seen from the TEM images, the resulting PPY-interpenetrated nanogels for all three thermoresponsive nanogels show spherical shape and low polydispersity (Fig. 4). As expected, the temperature-responsive properties of the nanogels remain unaffected by the semi-interpenetration process with VPTT of 33 °C (PPY/PNIPAM-dPG), 39.5 °C (PPY/Co-dPG) and 47 °C (PPY/PNIPMAM-dPG) (Table 1, Fig. S1). Interestingly, the size of the nanogels obtained from TEM is much smaller than the values obtained by DLS at swollen (25 °C) as well as shrunken (50 °C) state (Fig. 4D-F) indicating that the nanogels in shrunken state still contain a relatively high proportion of water.

Table 1
Characterization of different thermo-responsive nanogels semi-interpenetrated with PPY with varied molarities of the monomer swelling solution. Hydrodynamic size (d.nm), corresponding PDI values and VPTTs were measured by DLS (intensity distribution).

Py·HCl	PPY/PNIPAM-dPG			PPY/Co-dPG			PPY/PNIPMAM-dPG		
	25 °C	50 °C	VPTT (°C)	25 °C	50 °C	VPTT (°C)	25 °C	50 °C	VPTT (°C)
0.1 M	200 (0.162)	118 (0.062)	33.0	205 (0.119)	aggr.	–	241 (0.178)	aggr.	–
0.075 M	178 (0.191)	103 (0.097)	33.3	249 (0.167)	136 (0.074)	39.5	244 (0.213)	aggr.	–
0.05 M	176 (0.200)	103 (0.093)	33.3	197 (0.164)	97 (0.075)	39.5	204 (0.197)	147 (0.126)	47.0 °C

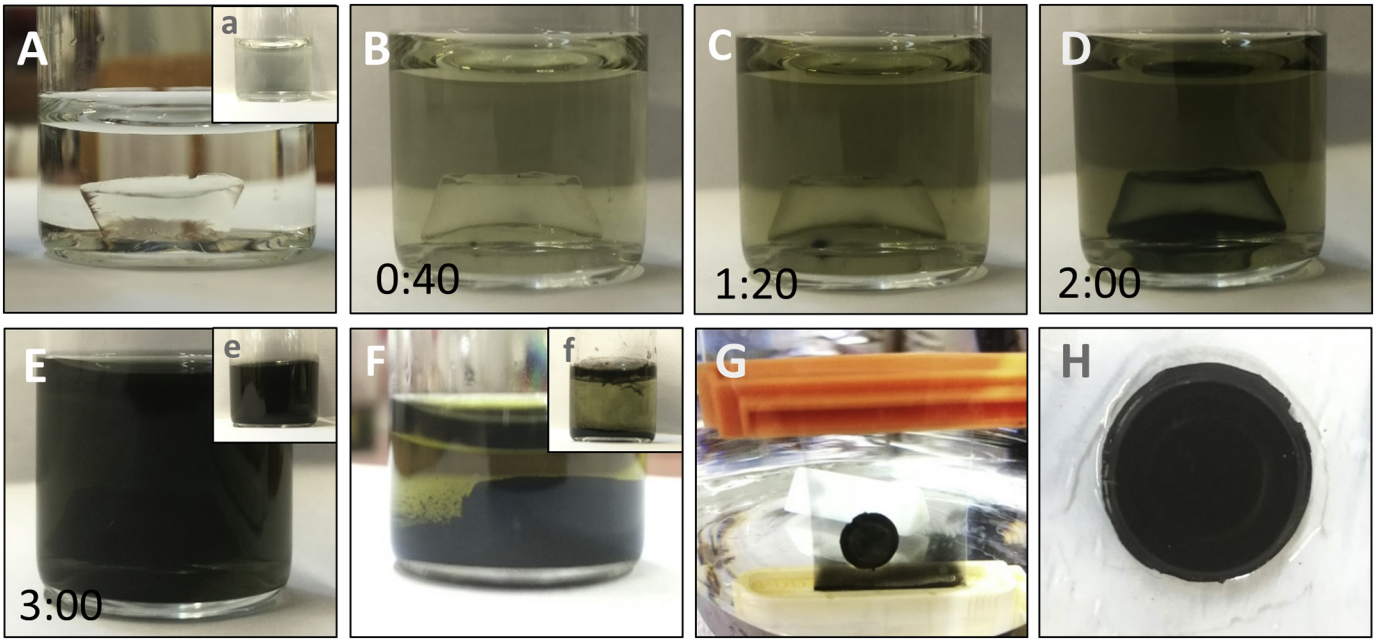

Fig. 2. PPY polymerization process inside a hydrogel. A) PNIPAM-dPG hydrogel swollen in Py·HCl solution, B)-E) polymerization of PPY in presence of a hydrogel indicated over time (min:sec) and F) appearance of the reaction mixture on the next day, G) semi-interpenetrated hydrogel in the dialysis bag, H) semi-interpenetrated hydrogel after purification. Insets a) e) and f) show the respective state in the polymerization process of PPY in the absence of a hydrogel.

3.2. Photothermal transducing ability and thermo-responsiveness under NIR trigger

Next, we investigated the ability of the formed PPY nanogels to transduce light of the NIR region into heat. For the application of the nanogels as drug delivery agents, stability of the particles is crucial. In addition, it is known that particles larger than 200 nm are more rapidly cleared from the body than smaller analogues [56]. We therefore chose PPY nanogels with sizes of a maximum of 200 nm and a PPY content assuring the retention of their stability upon heating (PPY/PNIPAM-dPG 0.1 M, PPY/Co-dPG 0.05 M, and PPY/PNIPMAM-dPG 0.05 M). The nanogel solutions were exposed to a NIR laser (785 nm, 500 mW) and temperature increase was monitored with an IR-camera. All nanogels showed concentration dependent heating reaching a temperature plateau after 120–150 s of irradiation (Fig. S2). The PPY/PNIPAM-dPG nanogels show increased heating performance as they contain more PPY, but all three nanogels increase the temperature of > 10 °C already at concentrations of 0.05 mg/mL or below (Fig. 5B). Repeated cycles of NIR exposure and cooling (Fig. 5C) demonstrate the excellent photostability of PPY in the interpenetrated nanogels.

To assess the nanogels' thermoresponsiveness during NIR irradiation and light-to-heat transduction, we measured the size of the nanogels immediately after NIR exposure. In all cases, we found a shrinkage of the nanogels and a reswelling to their original size within 5 min (Fig. 5D). For PPY/PNIPAM-dPG nanogels, even in low concentrations, temperatures higher than 50 °C, far above the VPTT, were reached during irradiation. For the other two nanogels, temperatures around their VPTT are reached at this concentration, and only at higher concentrations the solutions were heated above their transition temperature.

Surprisingly, we found that upon NIR irradiation the shrinkage of the nanogels is much more pronounced than only incubating them at

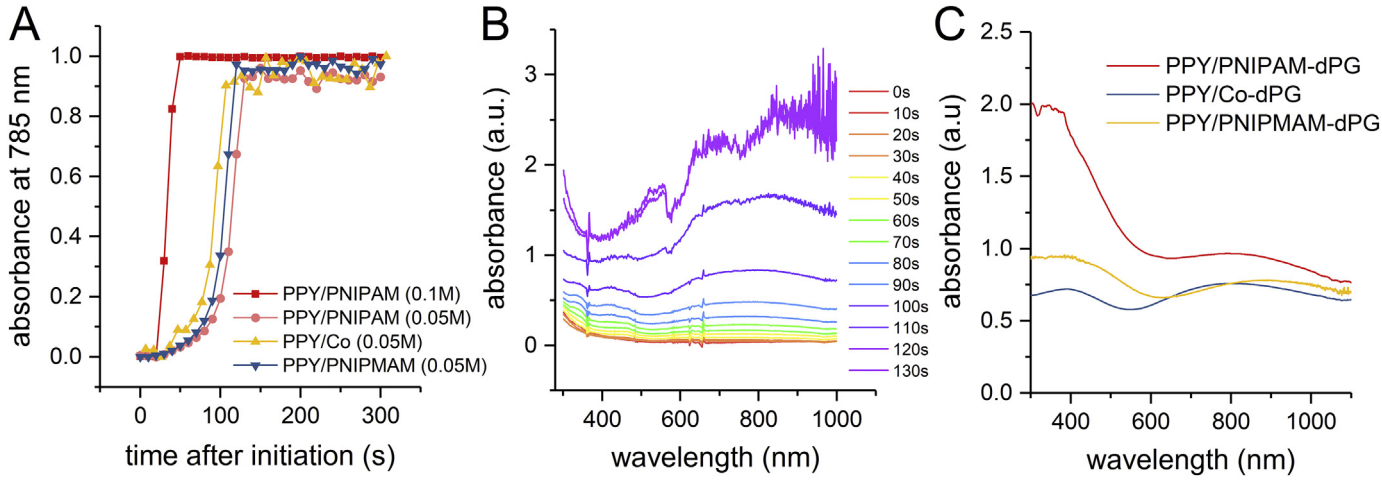

Fig. 3. Semi-interpenetration process studied by UV–Vis spectroscopy (A) Absorbance at 785 nm during first 5 min of polymerization, (B) UV-VIS spectra of PPY/PNIPMAM-dPG within the first 2 min after initiation, and (C) UV-VIS absorbance spectra of all three semi-interpenetrated PPY nanogels after purification in a concentration of 0.25 mg/mL.

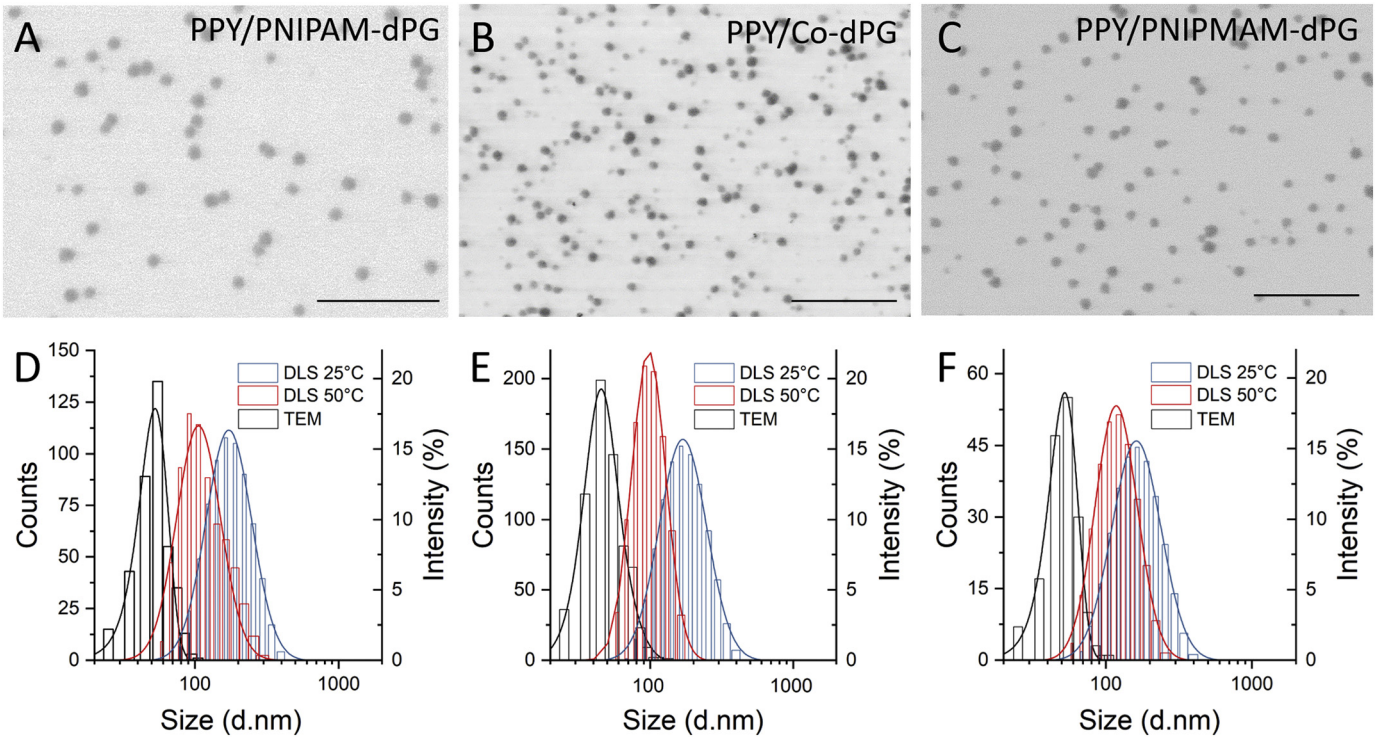

Fig. 4. Morphology of semi-interpenetrated PPY nanogels as studied by TEM and size comparison of in aqueous solution above and below the VPTT by DLS and in dry state by TEM. (A,D) PPY/PNIPAM-dPG, (B,E) PPY/Co-dPG and (C,F) PPY/PNIPMAM-dPG. Scale bar 500 nm.

the corresponding temperature (Fig. 5E). For instance, PPY/PNIPAM-dPG reach a temperature of 53.5 °C upon NIR (starting from 25 °C). The incubation at this temperature let the nanogels shrink about 42% to a relative size of 0.58 in comparison to their swollen state. In contrast, upon NIR exposure the nanogels even shrink about 68%. Also for PPY/Co-dPG and PPY/PNIPMAM-dPG the size decrease after NIR expose is more pronounced than induced by heating the whole solution. Triggered by NIR light, the shrinkage is increased about 9% (PPY/Co-dPG), respectively 18% (PPY/PNIPMAM-dPG) in comparison to the temperature-induced shrinkage in lower concentration of 0.1 mg/mL. This effect is even more pronounced at higher concentrations (0.25 mg/mL) with 17%, respectively 31% more shrinkage upon NIR exposure.

As in the lower concentration for both nanogels the photothermal conversion only causes a temperature increase close to the VPTT, we reason that the local temperature elevation in close vicinity to the PPY chains is likely much higher than measured by the IR camera in the whole solution. Thus, a collapse of the nanogels is induced even if the solution appeared to not reach temperatures high enough (above VPTT). This strong heating in close vicinity to the transducer is also reported for other photo-thermal agents like gold nanorods and gold-decorated upconversion nanoparticles along with a fast decay of the temperature with increasing distance to the particles surface [57,58].

Furthermore, the NIR irradiation seems to induce an additional shrinkage even over the maximal collapsed state caused by elevated temperature. In order to investigate this phenomenon, we irradiated nanogels while keeping the surrounding temperature as high as reached under NIR exposure at 25 °C. For example, PPY/PNIPAM-dPG nanogels were incubated at 53.5 °C as this was maximal temperature reached after 3 min of NIR exposure. As mentioned above, this temperature induce a size decrease of the nanogels about 42%. Then, the heated nanogel solution was additionally exposed to NIR and the size of the nanogels was measured immediately after 3 min of irradiation. We found an additional size decrease of 9% (Fig. 5E). Similar effects showing additional size reduction of 5–9% were found for PPY/Co-dPG and PPY/PNIPMAM-dPG when the incubation temperature was above the VPTT of the corresponding nanogel. Even stronger size reduction was found for PPY/Co-dPG (18%) and PPY/PNIPMAM-dPG (31%) nanogels in lower concentration, where the incubation temperature was close to the VPTT or below. Interestingly, the relative size reached for both nanogels under simultaneous application of temperature and NIR is similar and seems to be independent of the concentration. At both concentrations, the relative size is lower than what the heating of the solution above the transition temperature induce. Removing the NIR trigger, all nanogels re-swell to the size of the stage induced by the temperature applied (data not shown). We therefore conclude that upon local heat production under NIR exposure another portion of water is expelled from the nanogel procure an 'over-collapsed' state that only persists with the trigger applied.

Comparing the relative size of nanogels upon application of NIR we found that the 'over-collapse' is more prominent when the trigger is applied on swollen nanogels (incubated at 25 °C) and in concentrations reaching temperatures above the VPTT under irradiation than on collapsed nanogels (incubated above their VPTT). We correlate this to the formation of stabilizing, inter-polymeric hydrogen bonds, which were demonstrated to be present above the transition temperature for linear PNIPAM and PNIPMAM by Dybal and coworkers [59], acting against the additional size decrease when NIR exposure is applied on nanogels held above their VPTT.

Taken together, we can conclude that the semi-interpenetration of PPY into the thermo-responsive nanogels do not alter the general temperature-response of the resulting nanogels, but the local heat production upon photothermal conversion increase the shrinkage of the nanogels inducing the expulsion of additional interior water molecules.

3.3. Encapsulation and release of MTX

Having shown that our nanogels act as photothermal transducing agents and that the produced heat can be used to trigger the nanogels temperature response, we evaluated the performance of the nanogels as a drug delivery device. Therefore, we analysed the encapsulation and

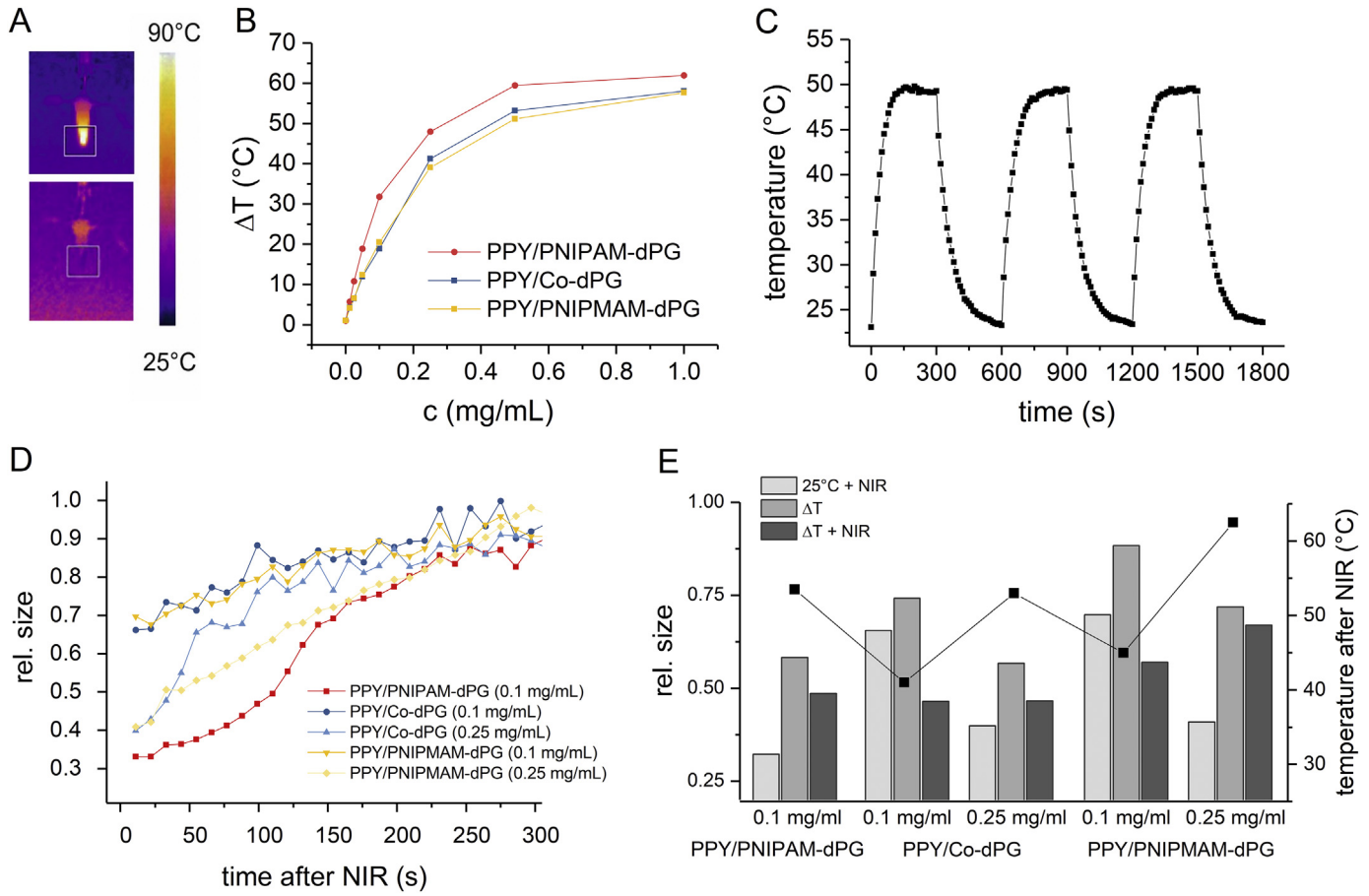

Fig. 5. Photothermal activity and thermo-responsiveness of the semi-interpenetrated PPY nanogels. (A) IR pictures of a sample during irradiation, (B) concentration dependent temperature difference reached after 5 min NIR irradiation, (C) three heating and cooling cycles of PPY/Co-dPG solution, (D) relative size of semi-interpenetrated nanogels after exposing to NIR laser for three minutes (t0) and reswelling after removal of NIR trigger, (E) comparison of relative size to swollen state after: 3 min NIR at r.t., at the corresponding temperature reached upon NIR (ΔT), and 3 min NIR at corresponding ΔT.

release properties using the anti-cancer drug methotrexate (MTX). Thermoresponsive nanogels have been proven to act as an excellent thermally triggered drug delivery device for proteins [41]. For the small molecule drug MTX however, we found low encapsulation efficiencies and fast, temperature independent release profiles for all three nanogels when they are not semi-interpenetrated with a second polymer (Fig. 6A,B). This is likely caused by a lack of beneficial interactions between the nanogels and MTX in combination with large mesh-sizes of the polymeric network, so that the small drug cannot be retained within the nanogels structure and its unhindered diffusion occurs. In contrast, we found about three fold higher encapsulation efficiencies for MTX in the semi-interpenetrated PPY nanogels up to 20 wt% (Fig. 6A). There are two factors which may cause these findings: first, upon interpenetration the nanogels' network is filled with PPY chains increasing the network density in each nanogel and thereby reducing their mesh size and restraining the free diffusion of the drug. Second, PPY is an electron-rich conjugated π-system which can interact with MTX molecules through π-π- and hydrophobic interactions and, with that, offer a driving force to MTX molecules to stay associated with the nanogels [31].

To test whether after semi-interpenetration the temperature-response of the nanogels has an impact on the release of the encapsulated MTX, release profiles of MTX from all PPY nanogels were assayed below and above their individual VPTT (Fig. 6C-E). Similar to the non-interpenetrated nanogels, we found no major influence of the temperature on the release profiles but a cumulative release of a maximum of 10–15% only, supporting the assumption of a strong interaction between PPY and MTX which keeps the drug preferably associated with the nanogels network. Remarkably, with the application of a NIR trigger, the release rate could be significantly promoted for all three PPY nanogels. We think that the main reason for this is the strong and local heating by the PPY chains able to loosen the interactions with the drug and in combination with the induced over-collapse of the nanogels network promoting its release.

3.4. Evaluation of cytotoxicity and therapeutic activity in vitro

Biocompatibility is a crucial factor for the application of new drug delivery materials. To obtain a first basis for an assessment, potential cytotoxic effects of all three semi-interpenetrated PPY nanogels was studied by MTT assay on A549 lung carcinoma cell line *in vitro*. For all three tested nanogels we found a very high tolerance of the cells for unloaded nanogels without reduction of cell viability up to concentrations of 1 mg/mL (Fig. S3A). The therapeutic activity of the nanogels was investigated in terms of their photothermal effect, delivery of the chemotherapeutic agent MTX and combinational effects of both. For drug loaded nanogels (10 wt% MTX), a reduction in cell viability similar to cells treated with free MTX is visible from nanogel concentrations of 15 μg/mL onwards, indicating that the loaded drug was successfully delivered from the nanogels in its active form (Fig. S3B, Fig. S4).

For evaluation of the photothermal activity and combination therapy with MTX, cells were incubated with the nanogels followed by irradiation for 7 min with a NIR laser. In order to gain comparability between the three nanogels systems, the applied nanogel concentrations were adjusted to have same absorbance properties at the

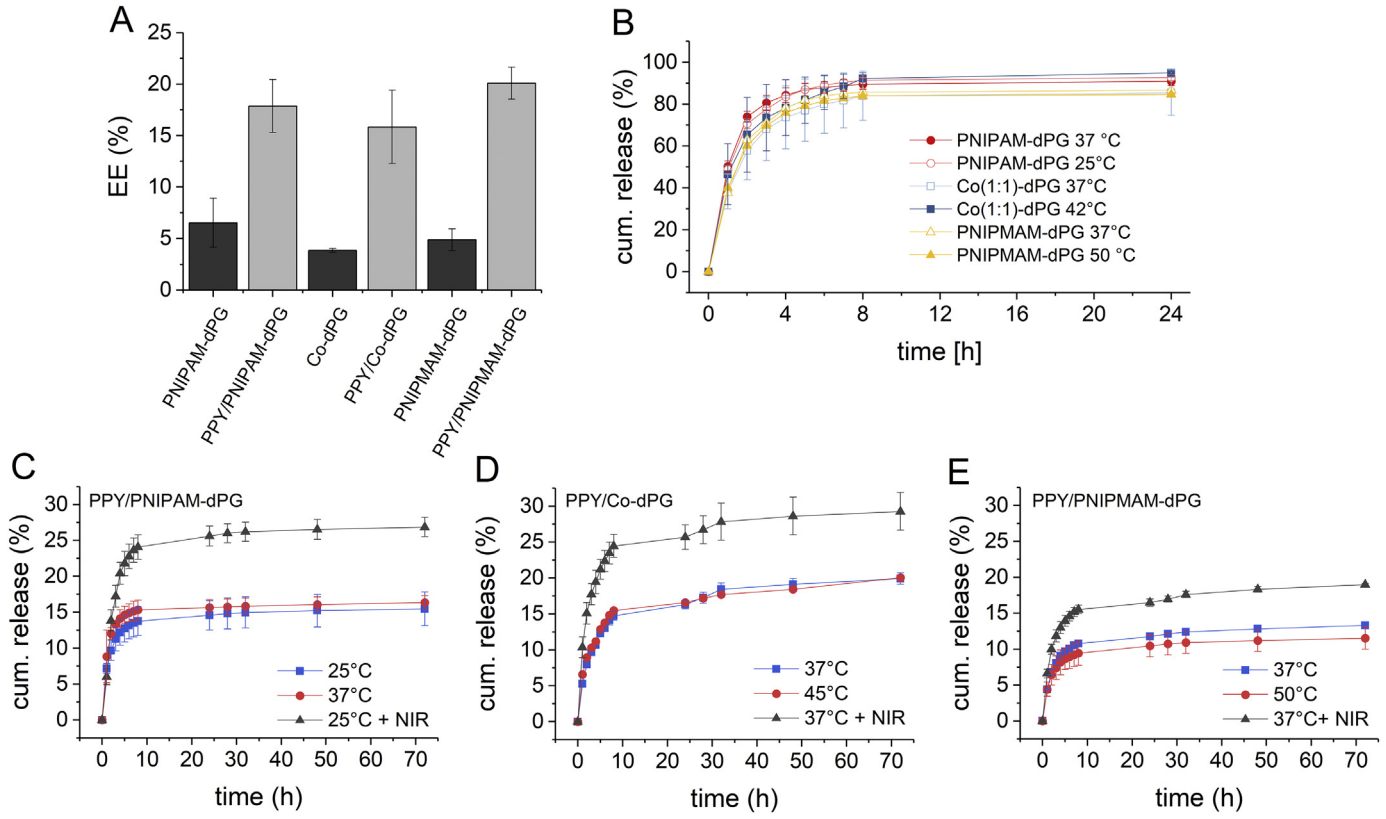

Fig. 6. (A) Encapsulation efficiency of MTX in non-interpenetrated and corresponding PPY nanogels, (B) release profiles of MTX above and below VPTT of the non-interpenetrated thermoresponsive nanogels, release profiles of semi-interpenetrated PPY nanogels: (C) PPY/PNIPAM, (D) PPY/Co, and (E) PPY/PNIPMAM each below and above the corresponding VPTT and upon NIR-irradiation with a NIR laser (785 nm, 500 mW) for 5 min every 2 h within the first 8 h.

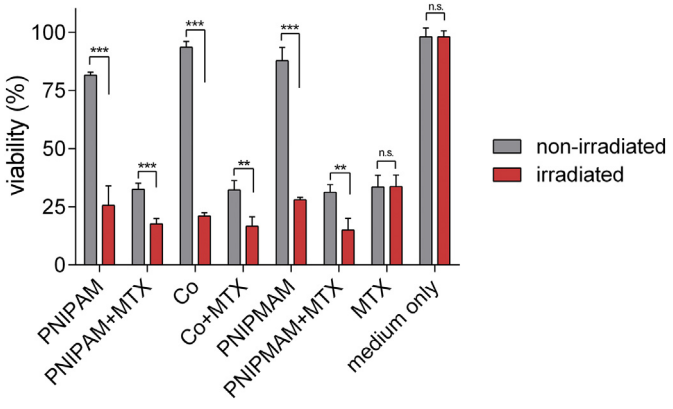

Fig. 7. Photothermal and combinational therapy *in vitro*. Cell viability of A549 lung carcinoma cell line determined by MTT assay incubated for 48 h with MTX loaded (10 wt%) and unloaded PPY nanogels with and without exposure to NIR laser (785 nm, 500 mW) for 7 min. Statistical significance was determined by multiple *t*-test analysis of variance deploying Holm-Sidak post-test with $*P \leq .05$ as significant, $**P \leq .01$ as very significant, and $*** P \leq .001$ as highly significant. All depicted values are mean ± standard error of the mean (SEM).

wavelength of irradiation (785 nm). Indeed, for all three nanogels, we see a similar photo-thermally induced reduction in cell viability to about 75–80% after irradiation and no reduction in the non-irradiated controls (Fig. 7).

For the MTX loaded nanogels, a combinational effect between chemotherapeutic activity of loaded MTX and photothermal heating by the nanogels is visible, appearing as significant additional reduction of the cell viability upon irradiation in comparison to the action of the delivered MTX alone. The NIR exposure of cells treated with only MTX did not cause this additional viability reduction proving that the increase in cell death is due to a combinational effect of MTX and the photothermal heating.

3.5. Evaluation of toxicity in vivo

Our results of *in vitro* efficiency suggest that all three nanogels are feasible candidates for application in a combinational anti-cancer therapy. As for all three PPY nanogels the thermo-responsiveness did not have an influence on the drug delivery profile, the main difference of the nanogels in an *in vivo* setting would be their hydration state. At systemic body temperature of 37 °C, semi-interpenetrated PPY/PNIPAM-dPG nanogels would be in a collapsed state whereas PPY/Co-dPG and PPY/PNIPMAM-dPG are still hydrated. Recently, we could demonstrate that the hydration state of thermo-responsive nanogels plays an important role in the formation of a protein corona which is known to be a key parameter for nanoparticles biodistribution profiles [44]. Therefore, we picked two out of the three nanogels of which one is in its collapsed state immediately upon administration (PPY/PNIPAM-dPG) and the other is still in a hydrated state, for evaluation in the mouse model. As hydrated nanogel we chose PPY/Co-dPG due to the higher MTX release rate under NIR exposure and slightly higher efficiency in the reduction of A549 cell viability by photothermal heating. First, tolerability of the nanogels in healthy mice was evaluated by following the body weight development after i.v. administration of first single injections with increasing doses (10–100 mg/kg) and then, five consecutive doses of the highest tolerated dose (100 mg/kg) over five days. For both tested nanogels, the body weight in the following two weeks was stable indicating no major toxicity effects (Fig. S5). In addition, the general behaviour of the mice was not altered indicating a good tolerability of the treatments. Afterwards, selected organs were

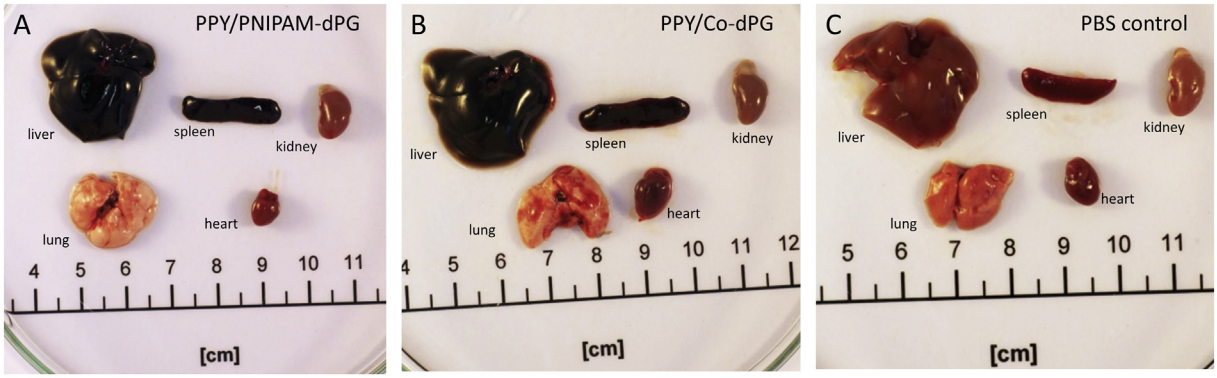

Fig. 8. Images of representative organs from mice treated intravenously with (A) PPY/PNIPAM-dPG and (B) PPY/Co-dPG for 5 consecutive days (100 mg/kg) and (C) untreated control (PBS, i.v.).

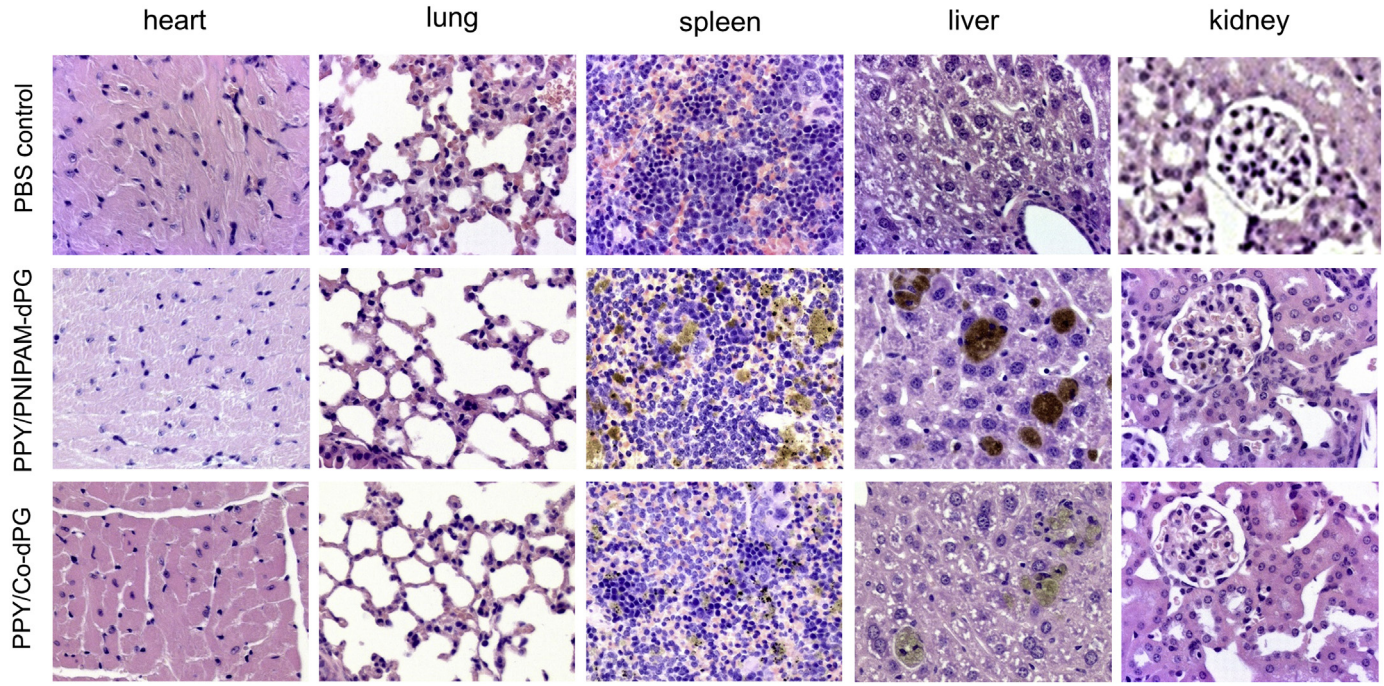

Fig. 9. H&E stained sections of selected organs of mice treated with PPY/PNIPMAM-dPG and PPY/Co-dPG nanogels in comparison to PBS control.

collected for histopathological examination. Macroscopically, particle accumulation mainly in the liver and spleen was visible as a black discoloration in these organs (Fig. 8). Apart from pigment storage seen in the spleen and liver, the histopathology revealed no specific inflammatory infiltrations or tissue damage (Fig. 9).

3.6. Biodistribution

The biodistribution profile of therapeutic actives is an important parameter to determine suitable dosing and study the fate of the carrier after systemic application. In the case of triggered drug delivery systems, we also need to determine the best time point for the application of the trigger, which is ideally characterized by an optimum accumulation of the carrier at the target site. Usually, biodistribution profiles are determined using radioactive or fluorescent labels for the particles of interest. In the case of PPY nanogels, fluorescent labeling is not feasible due to the strong absorbance of PPY resulting in strong quenching of the fluorescence signals. Radiolabels complicate the way of handling and the synthesis of the particles due to safety regulations working with radioactive substances. Both approaches anyhow require chemical modifications of the particles, which could influence the particles behaviour after administration. However, due to the photothermal transducing properties of the nanogels, they are ideal candidates to be used as PA signal enhancers usable as PA theranostic devices.

Thus, we assessed the nanogels accumulation by *ex vivo* imaging of organs excised from mice treated with the nanogels (5d x 100 mg/kg i.v.). MIPs (*cf.* page 10) over the x-y-plane of 3D PA images of the acquired organs at 800 nm are shown in Fig. 10A. The average image intensities (and standard deviations thereof) are shown in Fig. 10B. The strongest increase in PA image intensity compared to the control group (note the different scale bars in Fig. 10A) is observed for spleen and liver, which is in good agreement with the findings from macroscopic images that both nanogel systems mainly accumulate here (Fig. 8). Image intensity increases, albeit less pronounced, can also be seen in the kidney. By contrast, the PA image intensity measured in the heart and the lungs showed only minor changes indicating low to negligible particle accumulation.

Since the increase PA image intensity is based on the photothermal transducing ability of the nanogels, the *ex vivo* PA measurements were confirmed by measurements of the nanogel photothermal response. The organ samples imaged using PA tomography were illuminated with the

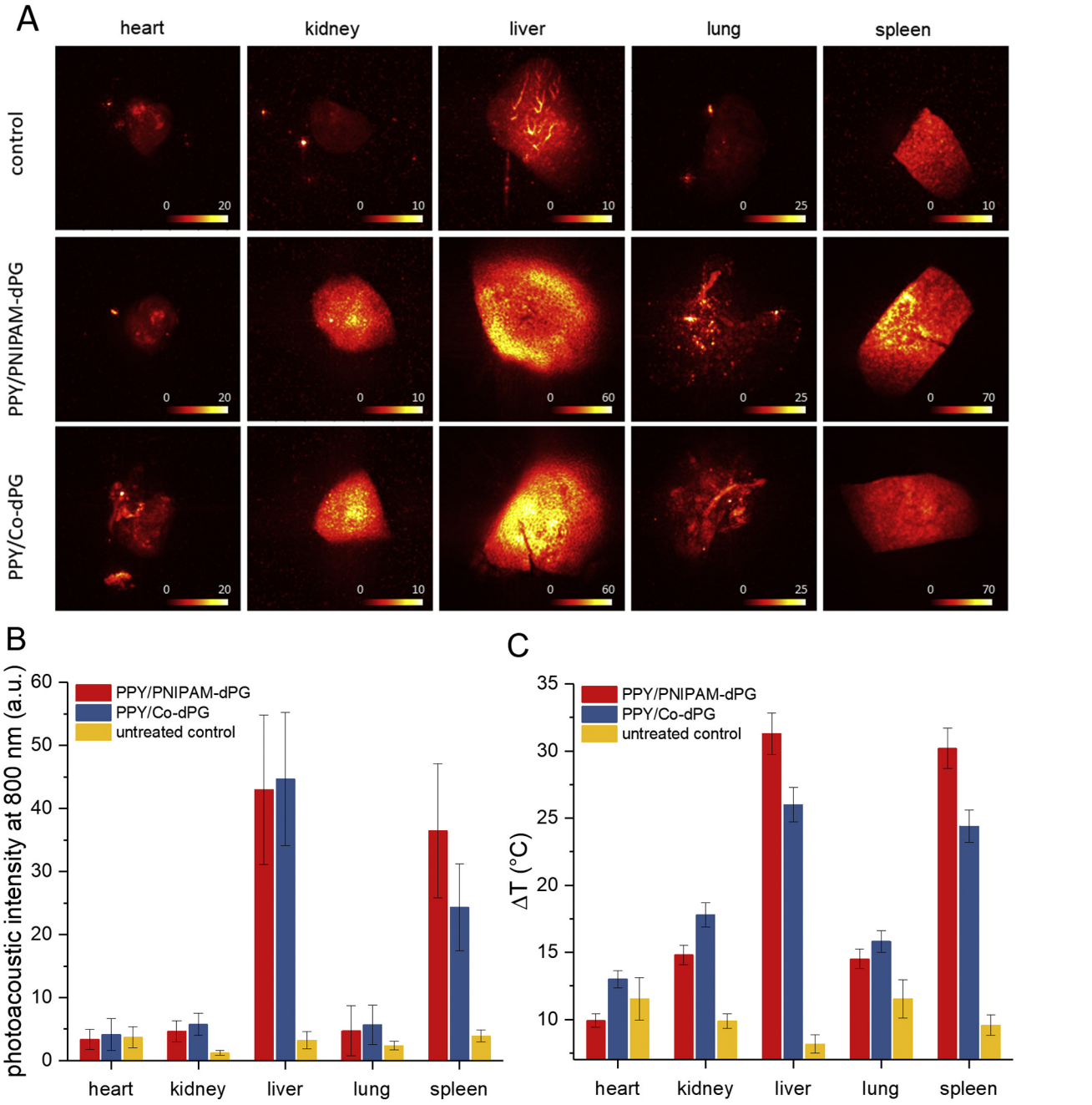

Fig. 10. (A) x-y MIPs of PA images of excised organs at 800 nm. Note that scale bars for intensity within organ groups are kept the same except for liver and spleen where the scale bar of the control organs were set much lower for better contrast. (B) Mean PA image intensity of excised, formalin fixed organs of a female nude mouse (NMRI, nu/nu) treated over five consecutive days with 100 mg/kg of PPY nanogels. (C) Photothermal response (max. ΔT after 5 min) of the same samples after irradiation with the output of a NIR lamp.

output of a NIR lamp and the resultant temperature increase was measured with an IR-camera. We found that the pattern of measured temperature increases agreed with the PA image intensity values, *i.e.* the highest values were found for both nanogels in the liver, closely followed by the spleen, and only slightly increased temperatures for the kidney and the lung (Fig. 10C).

These results motivated us to develop a setup for quantitative evaluation of the biodistribution profiles of our nanogels based on their photothermal response. In order to do so, we needed to fulfil two requirements: first, a maximized uniform distribution of particles in the investigated tissue to be able to compare reached temperature differences and second, a setup allowing to produce a calibration curve. We therefore decided to homogenize the organs and dilute them – either with PBS or with a nanogels containing solution for calibration purposes. With the established calibrations curves, weight prior and the volume after homogenisation, and the applied dilution factor, we were able to calculate quantitative biodistribution profiles with accuracy down to 50 µg/mL using a NIR lamp and even lower to values of 12.5 µg/mL using a NIR laser (Fig. S6). The resulting profiles for both nanogels directly after the last treatment or at the end of the study are shown in Fig. S7. These profiles were meant for method validation and interpretation of the results can only serve as first indication due to the low number of mice evaluated ($n = 1$ for d6 and $n = 2$ for d21). In accordance with the photoacoustic measurement, main particle accumulation is detected in liver and spleen. Interestingly, emphasis of the organ weight, reflecting particle density in the organ sample, slightly

higher values are observed in the spleen than in the liver. In addition, it seems that the particles segregate from the liver over time, showing much lower values at d21 than directly after treatment.

In general, for polymeric nanocarriers such biodistribution pattern, exhibiting the majority of particles accumulated in the liver and the spleen, is quite common. This is due to the particles clearance by the reticuloendothelial system (RES). Induced by the binding of opsonins to the nanoparticles surface, phagocytes such as macrophages can recognise the nanoparticles, internalize them and start to secret enzymes and other oxidative-reactive chemical factors to break down the particles. However, most polymeric nanoparticles cannot be degraded significantly by this process. This results in particular for high molecular weight particles in a storage in the organs of the RES; the liver and the spleen [56,60].

In order to achieve that polymeric carriers reach their target and deliver their cargos prior to the recognition by the RES, several factors are commonly addressed. Foremost, the reduction of the opsonisation of the particles is tackled through introduction of stealth properties to the surface of the nanoparticles preventing the absorption of proteins. Here, most commonly a surface functionalization with PEG is performed. The reduction of protein binding to PEGylated particles delays the particle recognition by the RES and increases their blood circulation time. This allows sufficient accumulation of particles at the target site, *e.g.* using the EPR effect [30,61]. Beside the surface stealth properties, additionally the size of the nanoparticles and their hydrophilic-hydrophobic character are known to influence the opsonisation process [56,62]. Independent of stealth properties, it was found that particles with sizes below 200 nm have greater circulations times and are more slowly cleared from the body. In addition, the opsonisation of hydrophobic particles, as compared to hydrophilic particles, has been shown to occur more quickly [56,60,63].

With the new method in hand, we thus aimed to investigate the ability of our nanogels to accumulate at the tumor site and prolong the circulation in the blood. The effect of the hydration state on the biodistribution additionally can be investigated with the two nanogels PPY/PNIPAM-dPG and PPY/Co-dPG being in different hydration state upon administration.

Therefore, biodistribution profiles after single i.v. dosage (100 mg/kg) in tumor bearing mice (A549/NMRI: nu/nu (f)) were employed 2 h, 12 h, and 48 h after the injection. As can be seen from Fig. S8 for both nanogels, the majority of the particles can be found in the liver whereas particle density was found to be similar with 50–80%ID/g in the liver and spleen (Fig. 11A). Both nanogels show an increase in particle density in the liver from 2 h to 12 h and then start to segregate slowly, whereas highest particle density in the spleen is already reached after 2 h with a continuous decrease afterwards. Interestingly, in the other organs (heart, kidney, lung and, tumor) major differences between the two nanogel systems are visible. PPY/Co-dPG nanogels are found in heart, lung and kidney in relatively high concentrations after 2 h, with decreasing concentrations in all organs over time, indicating that the particles are still circulating in the bloodstream in the first hours after injection. In contrast, PPY/PNIPAM-dPG nanogels show only notable presence in the lung 2 h post injection and are already almost completely cleared therefrom after 12 h.

To our surprise, we could detect only the PPY/Co-dPG nanogels, not however the PPY/PNIPAM-dPG nanogels in the tumor site with highest accumulation 48 h after treatment (Fig. 11B). We assume this could be due to the different hydration state of the nanogels. PPY/PNIPAM-dPG nanogels are in their collapsed state at systemic temperatures of 37 °C immediately after injection whereas PYY/Co-dPG nanogels are still hydrated. The collapse of the nanogels induce three major changes which may be responsible for the different behaviour upon administration: First, the hydrophilic-hydrophobic balance is shifted to a more hydrophobic state with a pronounced polymer-polymer interaction and less hydration; second, upon the collapse of the thermo-responsive network a higher ratio of semi-interpenetrating polymer PPY will be located outside or on the nanogels surface and reduce the presence of dPG acting as stabilizing agent; and third the size of the nanogels drops significantly down from 200 nm to 120 nm. All three factors are known to be important as the nanogels surface properties prevent opsonisation in the blood and are important to reduce recognition by the reticuloendothelial system (RES) leading to prolonged blood circulation time which is a major factor for passive targeting of tumor tissue [45,56,64–66]. PPY/Co-dPG nanogels reach an accumulation of 5% ID/g which corresponds to a particle concentration of 70 μg/cm^3 tumor volume equivalent to a temperature increase up to 41–42 °C under NIR irradiation with the NIR laser. This temperature may be feasible for hyperthermia applications where increased temperature exposure is kept for several hours [2], but are still too low for tumor ablation with short application of the external NIR irradiation. Alltogether, we can conclude that PPY/PNIPAM-dPG nanogels are only feasible candidates for i.t. applications and PPY/Co nanogels need higher dosed or several times administered in order to increase the concentration at the tumor site for photothermal ablation.

3.7. Therapeutic activity in vivo

We evaluated the antitumoral activity of the PPY nanogels in several

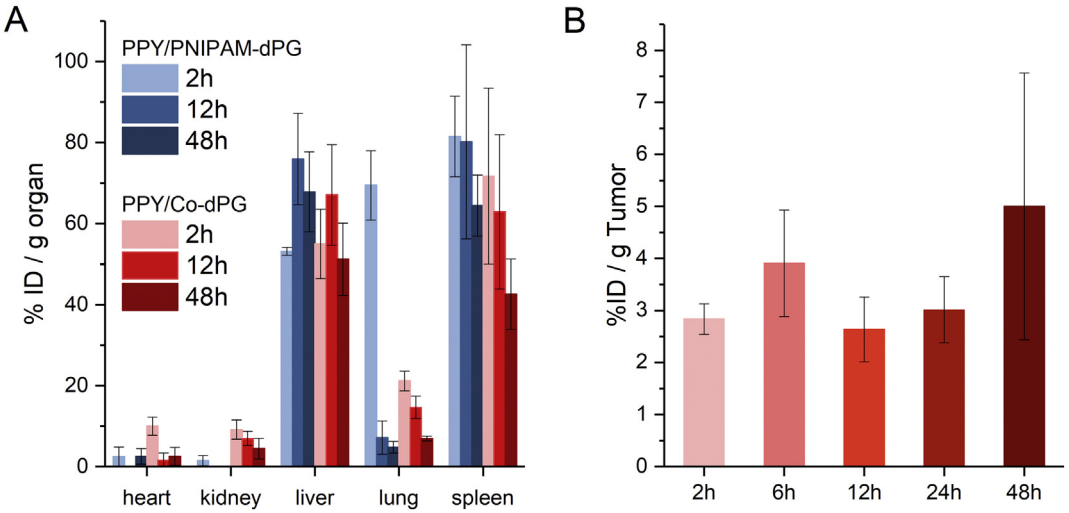

Fig. 11. (A) Biodistribution profile of PPY/PNIPAM-dPG and PPY/Co-dPG nanogels shown as percent of injected dose (%ID) per g organ after 2 h, 12 h, 48 h post injection and (B) accumulation of PPY/Co-dPG nanogels in the tumor site at 2 h, 6 h, 12 h, 24 h, and 48 h after i.v. injection.

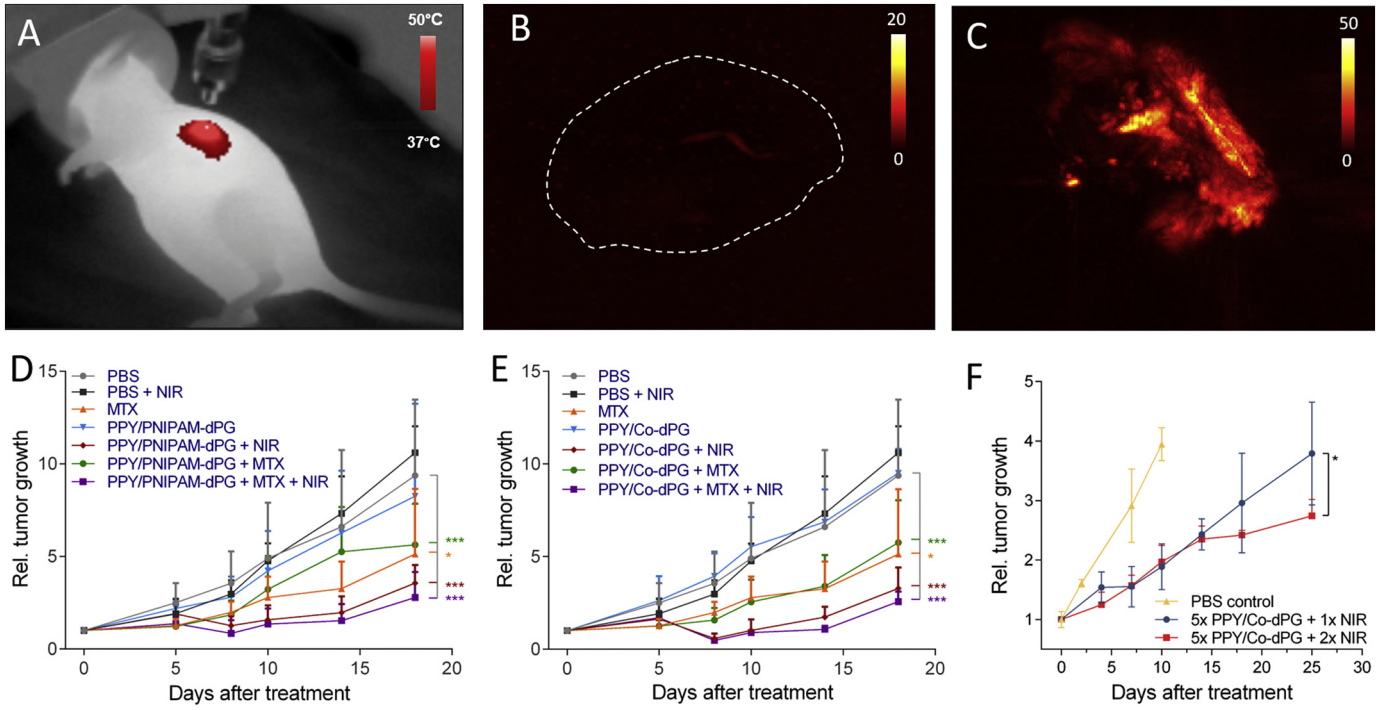

Fig. 12. (A) IR image of a mice under NIR irradiation with i.t. injected nanogels, (B) MIP of photoacoustic image of an untreated control tumor *ex vivo* and (C) MIP of photoacoustic image of a tumor after injection of nanogels and 5 min NIR irradiation (30 µL, 10 mg/mL) *ex vivo*. (D-E) Rel. tumor growth over time of mice treated i.t. with MTX loaded and bare PPY/PNIPAM-dPG nanogels (D) and PPY/Co-dPG nanogels (E) with and without exposure to NIR for 5 min. PBS treated mice with and without NIR exposure and MTX treated mice served as control. (F) Rel. tumor growth over time after i.v. administration of 5 consecutive doses (100 mg/kg) of PPY/Co-dPG and exposure to NIR (5 min) 48 h after last injection and with additional irradiation after the third injection. Statistical significance between rel. Tumor volumes at the endpoint (d18) of the studies was determined by two-way ANOVA analysis of variance with $^{*}P \leq .05$ as significant, $^{**}P \leq .01$ as very significant, and *** $P \leq .001$ as highly significant. All depicted values are mean ± standard error of the mean (SEM).

manners. First, the nanogels were administered i.t. in order to study the photothermal effect of a known concentration at the tumor site and combinational effect with the loaded drug. Therefore, A549 xenograft tumor bearing mice were treated intratumorally with 300 µg of each nanogel and irradiated with the NIR laser for 5 min.

The temperature increase during irradiation was monitored using an IR camera (Fig. 12A) proving that the temperature increase is very local only at the tumor site with temperature of the surrounding tissue of 36–37 °C. For both nanogels, strong heating of the tumor site upon NIR exposure was recorded reaching temperatures > 50 °C. These high temperatures caused skin burns in the mice after the treatment which however healed over the following 10 days (Fig. S9). In addition, we assessed the particle distribution within the tumors after the treatment by taking photoacoustic images (*ex vivo*, one tumor per group). In comparison to the untreated control (Fig. 12B) PA intensities are increased within the whole tumor indicating a distribution of particles, but highest values are found close to the puncture site reflecting higher concentration of nanogels here (Fig. 12C).

All assayed treatment modalities were found to be well tolerated reflected in no major BW changes over the whole period of the study (Fig. S10). For both nanogels, PTT significantly inhibited the tumor growth, whereas non-irradiated controls did not show any effect on the tumor size (Fig. 12D,E). In good agreement with the results obtained *in vitro,* the drug loaded nanogels slowed down tumor progression in a similar manner to the free drug demonstrating the ability of nanogels to deliver MTX. The combination of PTT and chemotherapeutic action of MTX result in reduced tumor regrowth, even though it has to be mentioned that the high efficiency of the PTT alone impede measurements of significant differences.

We therefore performed tumor inhibition studies limiting the temperature at the tumor site upon NIR exposure to 45 °C by reduction of the laser power, but found that neither 5 min nor a prolonged irradiation time of 15 min had a major influence on tumor growth (Fig. S11). Similar findings where observed by Liu et al. with only minimal growth inhibition of tumors of a breast cancer cell line 4 T1 implanted on mice with local temperature increases to 44 °C [31]. By the same authors, efficient tumor reduction by PTT was only achieved with temperature increases of the tumor to 47–48 °C.

As biodistribution profiles revealed that only PPY/Co-dPG nanogels are feasible candidates for i.v. administration and knowing that high temperatures are required for photothermal ablation of cancer cells, we decided to try to increase the intratumoral concentration of the PPY/Co-dPG nanogels by applying several i.v. doses in a consecutive manner. In addition, we were interested if several NIR irradiations will increase the efficiency of the treatment. Indeed, the development of the tumor volume with a single or two expositions to NIR revealed that both treatments are able to slow down tumor growth with slightly higher effectiveness of the inhibition upon several NIR expositions (Fig. 12F). Together with the result from i.t. administration, we would expect better performance of tumor inhibition with drug loaded nanogels, nevertheless for future work additional active targeting moieties or combination with EPR augmenting agents need to be considered.

4. Conclusion

Stabilization and water dispersion of NIR-transducing polymer PPY could be successfully achieved by semi-interpenetration of thermo-responsive nanogels. The thermo-responsive network was able to stabilize the PPY and prevent aggregation over long time. The resulting semi-interpenetrated PPY nanogels still exhibit the same VPTT as their thermo-responsive non-interpenetrated analogues and act as excellent photothermal transducer with high photostability. The photothermal transducing abilities of the nanogels can be used for PA contrast enhancement, which allows determination of the nanogels distribution

after administration *ex vivo*. In addition, with the PA measurements we validated a new method for the assessment of biodistribution *ex vivo* using the photothermal response of the nanogels with accuracy down to concentrations of 12.5 μg/mL, allowing label free detection.

With the non-interpenetrated thermo-responsive nanogels, a similar temperature-triggered release profile as obtained in earlier work for large proteins could not be observed, which is likely due to the small molecular weight of the chemotherapeutic drug MTX. However, we could show that semi-interpenetration of PPY into these nanogels resulted in threefold higher encapsulation efficiencies and increased release rates were found upon NIR exposure.

The combinational effect of photothermal ablation and chemotherapy with almost complete tumor elimination could be demonstrated *in vitro* and *in vivo* upon i.t administration. Due to the collapse of PNIPAM based nanogels at body temperature of 37 °C, these nanogels turned out to be only feasible for i.t. administration. In contrast, PPY/Co nanogels are able to accumulate sufficiently with several i.v. injections and were able to slow down tumor growth. Further fine-tuning of these nanogels for enhanced passive as well as active targeting is currently under investigation. In addition, other chemotherapeutic actives of larger size for temperature induced release behaviour are of interest for future studies.

Data availability

The raw data required to reproduce these findings are available upon request to the corresponding author.

Declaration of Competing Interest

The authors declare no competing financial interest.

Acknowledgements

We gratefully acknowledge financial support from Bundesministerium für Bildung und Forschung (BMBF), Germany, NanoMatFutur Award 13N12561, Deutsche Forschungsgemeinschaft (DFG), Germany, project grant LA3273/1-1, and the IKERBASQUE-Basque Foundation for Science. We acknowledge Emanuel Glitscher and Julian Bergueiro for the measurement of the TEM images. Sincere thanks also to Sebastian Heintze for help with organ sampling and cell assays.

Appendix A. Supplementary data

Synthetic details for acrylated dPG, ^{1}H NMR spectra of thermo-responsive nanogels, VPTT diagrams, PTR curves of PPY nanogels in different concentrations, Cytotoxicity of nanogels and MTX loaded nanogels, BW change upon nanogel administration in healthy and tumor bearing mice. Supplementary data to this article can be found online at https://doi.org/10.1016/j.jconrel.2019.08.035.

References

[1] Y. Liu, P. Bhattarai, Z. Dai, X. Chen, Photothermal therapy and photoacoustic imaging via nanotheranostics in fighting cancer, Chem. Soc. Rev. 48 (2019) 2053–2108.
[2] D. Jaque, L. Martinez Maestro, B. del Rosal, P. Haro-Gonzalez, A. Benayas, J.L. Plaza, E. Martin Rodriguez, J. Garcia Sole, Nanoparticles for photothermal therapies, Nanoscale 6 (16) (2014) 9494–9530.
[3] M. Wang, Emerging multifunctional NIR photothermal therapy systems based on polypyrrole nanoparticles, Polymers 8 (10) (2016) 373.
[4] Z. Li, H. Huang, S. Tang, Y. Li, X.-F. Yu, H. Wang, P. Li, Z. Sun, H. Zhang, C. Liu, P.K. Chu, Small gold nanorods laden macrophages for enhanced tumor coverage in photothermal therapy, Biomaterials 74 (2016) 144–154.
[5] J. Kim, S. Park, J.E. Lee, S.M. Jin, J.H. Lee, I.S. Lee, I. Yang, J.-S. Kim, S.K. Kim, M.-H. Cho, T. Hyeon, Designed fabrication of multifunctional magnetic gold nanoshells and their application to magnetic resonance imaging and photothermal therapy, Angew. Chem. 118 (46) (2006) 7918–7922.
[6] P. Botella, Í. Ortega, M. Quesada, R.F. Madrigal, C. Muniesa, A. Fimia, E. Fernández, A. Corma, Multifunctional hybrid materials for combined photo and chemotherapy of cancer, Dalton Trans. 41 (31) (2012) 9286–9296.
[7] H. Park, J. Yang, J. Lee, S. Haam, I.-H. Choi, K.-H. Yoo, Multifunctional nanoparticles for combined doxorubicin and photothermal treatments, ACS Nano 3 (10) (2009) 2919–2926.
[8] C. Liang, S. Diao, C. Wang, H. Gong, T. Liu, G. Hong, X. Shi, H. Dai, Z. Liu, Tumor metastasis inhibition by imaging-guided photothermal therapy with single-walled carbon nanotubes, Adv. Mater. 26 (32) (2014) 5646–5652.
[9] L. Feng, K. Li, X. Shi, M. Gao, J. Liu, Z. Liu, Smart pH-responsive nanocarriers based on nano-graphene oxide for combined chemo- and photothermal therapy overcoming drug resistance, Adv. Healthc. Mater. 3 (8) (2014) 1261–1271.
[10] D. Chen, C. Wang, X. Nie, S. Li, R. Li, M. Guan, Z. Liu, C. Chen, C. Wang, C. Shu, L. Wan, Photoacoustic imaging guided near-infrared photothermal therapy using highly water-dispersible single-walled carbon nanohorns as theranostic agents, Adv. Funct. Mater. 24 (42) (2014) 6621–6628.
[11] Z. Zha, X. Yue, Q. Ren, Z. Dai, Uniform polypyrrole nanoparticles with high photothermal conversion efficiency for photothermal ablation of cancer cells, Adv. Mater. 25 (5) (2013) 777–782.
[12] K. Yang, H. Xu, L. Cheng, C. Sun, J. Wang, Z. Liu, In vitro and in vivo near-infrared photothermal therapy of cancer using polypyrrole organic nanoparticles, Adv. Mater. 24 (41) (2012) 5586–5592.
[13] M. Chen, X. Fang, S. Tang, N. Zheng, Polypyrrole nanoparticles for high-performance in vivo near-infrared photothermal cancer therapy, Chem. Commun. 48 (71) (2012) 8934–8936.
[14] J. Yang, J. Choi, D. Bang, E. Kim, E.K. Lim, H. Park, J.S. Suh, K. Lee, K.H. Yoo, E.K. Kim, Y.M. Huh, S. Haam, Convertible organic nanoparticles for near-infrared photothermal ablation of cancer cells, Angew. Chem. Int. Ed. 50 (2011) 441–444.
[15] E.I. Yslas, L.E. Ibarra, M.A. Molina, C. Rivarola, C.A. Barbero, M.L. Bertuzzi, V.A. Rivarola, Polyaniline nanoparticles for near-infrared photothermal destruction of cancer cells, J. Nanopart. Res. 17 (10) (2015) 389.
[16] M. Molina, S. Wedepohl, M. Calderón, Polymeric near-infrared absorbing dendritic nanogels for efficient in vivo photothermal cancer therapy, Nanoscale 8 (2016) 5852–5856.
[17] Y. Zhou, Y. Hu, W. Sun, B. Zhou, J. Zhu, C. Peng, M. Shen, X. Shi, Polyaniline-loaded γ-polyglutamic acid nanogels as a platform for photoacoustic imaging-guided tumor photothermal therapy, Nanoscale 9 (34) (2017) 12746–12754.
[18] H. Gong, L. Cheng, J. Xiang, H. Xu, L. Feng, X. Shi, Z. Liu, Near-infrared absorbing polymeric nanoparticles as a versatile drug carrier for cancer combination therapy, Adv. Funct. Mater. 23 (48) (2013) 6059–6067.
[19] L. Cheng, K. Yang, Q. Chen, Z. Liu, Organic stealth nanoparticles for highly effective in vivo near-infrared photothermal therapy of cancer, ACS Nano 6 (6) (2012) 5605–5613.
[20] T. Aoki, M. Tanino, K. Sanui, N. Ogata, K. Kumakura, Secretory function of adrenal chromaffin cells cultured on polypyrrole films, Biomaterials 17 (20) (1996) 1971–1974.
[21] L. Ghasemi-Mobarakeh, M.P. Prabhakaran, M. Morshed, M.H. Nasr-Esfahani, H. Baharvand, S. Kiani, S.S. Al-Deyab, S. Ramakrishna, Application of conductive polymers, scaffolds and electrical stimulation for nerve tissue engineering, J. Tissue Eng. Regen. Med. 5 (4) (2011) e17–e35.
[22] R. Balint, N.J. Cassidy, S.H. Cartmell, Conductive polymers: towards a smart biomaterial for tissue engineering, Acta Biomater. 10 (6) (2014) 2341–2353.
[23] P.M. George, A.W. Lyckman, D.A. LaVan, A. Hegde, Y. Leung, R. Avasare, C. Testa, P.M. Alexander, R. Langer, M. Sur, Fabrication and biocompatibility of polypyrrole implants suitable for neural prosthetics, Biomaterials 26 (17) (2005) 3511–3519.
[24] E. Fernández, P. Botella, Biotolerability of Intracortical microelectrodes, Adv. Biosyst. 2 (1) (2018) 1700115.
[25] A. Fahlgren, C. Bratengeier, A. Gelmi, C.M. Semeins, J. Klein-Nulend, E.W.H. Jager, A.D. Bakker, Biocompatibility of polypyrrole with human primary osteoblasts and the effect of dopants, PLoS One 10 (7) (2015) e0134023.
[26] D.D. Ateh, H.A. Navsaria, P. Vadgama, Polypyrrole-based conducting polymers and interactions with biological tissues, J. R. Soc. Interface 3 (11) (2006) 741–752.
[27] M. Chen, X. Fang, S. Tang, N. Zheng, Polypyrrole nanoparticles for high-performance in vivo near-infrared photothermal cancer therapy, Chem. Commun. 48 (2012) 8934–8936.
[28] Y. Tian, J. Zhang, S. Tang, L. Zhou, W. Yang, Polypyrrole composite nanoparticles with morphology-dependent photothermal effect and immunological responses, Small 12 (6) (2016) 721–726.
[29] Z. Zha, Z. Deng, Y. Li, C. Li, J. Wang, S. Wang, E. Qu, Z. Dai, Biocompatible polypyrrole nanoparticles as a novel organic photoacoustic contrast agent for deep tissue imaging, Nanoscale 5 (10) (2013) 4462–4467.
[30] X. Liang, Y. Li, X. Li, L. Jing, Z. Deng, X. Yue, C. Li, Z. Dai, PEGylated polypyrrole nanoparticles conjugating gadolinium chelates for dual-modal mri/photoacoustic imaging guided photothermal therapy of cancer, Adv. Funct. Mater. 25 (9) (2015) 1451–1462.
[31] C. Wang, H. Xu, C. Liang, Y. Liu, Z. Li, G. Yang, L. Cheng, Y. Li, Z. Liu, Iron oxide @ polypyrrole nanoparticles as a multifunctional drug carrier for remotely controlled cancer therapy with synergistic antitumor effect, ACS Nano 7 (8) (2013) 6782–6795.
[32] Y. Zhou, Y. Hu, W. Sun, S. Lu, C. Cai, C. Peng, J. Yu, R. Popovtzer, M. Shen, X. Shi, Radiotherapy-sensitized tumor photothermal ablation using γ-polyglutamic acid nanogels loaded with polypyrrole, Biomacromolecules 19 (6) (2018) 2034–2042.
[33] Y. Wang, Y. Xiao, R. Tang, Spindle-like polypyrrole hollow nanocapsules as multifunctional platforms for highly effective chemo–photothermal combination therapy of cancer cells in vivo, Chem. Eur. J. 20 (37) (2014) 11826–11834.
[34] Z. Meng, X. Chen, Z. Liu, S. Chen, N. Yu, P. Wei, Z. Chen, M. Zhu, NIR-laser-

triggered smart full-polymer nanogels for synergic photothermal−/chemo-therapy of tumors, RSC Adv. 6 (93) (2016) 90111–90119.
[35] K.S. Soni, S.S. Desale, T.K. Bronich, Nanogels: an overview of properties, biomedical applications and obstacles to clinical translation, J. Control. Release 240 (2016) 109–126.
[36] M. Kar, M. Molina, M. Calderón, How are we applying nanogel composites in biomedicine? Nanomedicine 12 (14) (2017) 1627–1630.
[37] A.J. Sivaram, P. Rajitha, S. Maya, R. Jayakumar, M. Sabitha, Nanogels for delivery, imaging and therapy, Wiley Interdiscip. Rev. Nanomed. Nanobiotechnol. 7 (4) (2015) 509–533.
[38] A.V. Kabanov, S.V. Vinogradov, Nanogels as pharmaceutical carriers: finite networks of infinite capabilities, Angew. Chem. Int. Ed. Engl. 48 (30) (2009) 5418–5429.
[39] M. Molina, M. Asadian-Birjand, J. Balach, J. Bergueiro, E. Miceli, M. Calderon, Stimuli-responsive nanogel composites and their application in nanomedicine, Chem. Soc. Rev. 44 (17) (2015) 6161–6186.
[40] F. Sultana, M. Imran-Ul-Haque Manirujjaman, M. Arafat, S. Sharmin, An overview of nanogel drug delivery system, J. Appl. Pharm. Sci. 3 (8) (2013) 95–105.
[41] L.E. Theune, R. Charbaji, M. Kar, S. Wedepohl, S. Hedtrich, M. Calderón, Critical parameters for the controlled synthesis of nanogels suitable for temperature-triggered protein delivery, Mater. Sci. Eng. C 100 (2019) 141–151.
[42] M. Witting, M. Molina, K. Obst, R. Plank, K.M. Eckl, H.C. Hennies, M. Calderón, W. Frieß, S. Hedtrich, Thermosensitive dendritic polyglycerol-based nanogels for cutaneous delivery of biomacromolecules, Nanomedicine 11 (5) (2015) 1179–1187.
[43] S. Abbina, S. Vappala, P. Kumar, E.M.J. Siren, C.C. La, U. Abbasi, D.E. Brooks, J.N. Kizhakkedathu, Hyperbranched polyglycerols: recent advances in synthesis, biocompatibility and biomedical applications, J. Mater. Chem. B 5 (47) (2017) 9249–9277.
[44] E. Miceli, B. Kuropka, C. Rosenauer, E.R.O. Blanco, L.E. Theune, M. Kar, C. Weise, S. Morsbach, C. Freund, M. Calderón, Understanding the elusive protein corona of thermoresponsive nanogels, Nanomedicine 13 (20) (2018) 2657–2668.
[45] J. Khandare, M. Calderon, N.M. Dagia, R. Haag, Multifunctional dendritic polymers in nanomedicine: opportunities and challenges, Chem. Soc. Rev. 41 (7) (2012) 2824–2848.
[46] S. Ritz, S. Schöttler, N. Kotman, G. Baier, A. Musyanovych, J. Kuharev, K. Landfester, H. Schild, O. Jahn, S. Tenzer, V. Mailänder, Protein corona of nanoparticles: distinct proteins regulate the cellular uptake, Biomacromolecules 16 (4) (2015) 1311–1321.
[47] K. Obst, G. Yealland, B. Balzus, E. Miceli, M. Dimde, C. Weise, M. Eravci, R. Bodmeier, R. Haag, M. Calderón, N. Charbaji, S. Hedtrich, Protein corona formation on colloidal polymeric nanoparticles and polymeric Nanogels: impact on cellular uptake, toxicity, immunogenicity, and drug release properties, Biomacromolecules 18 (6) (2017) 1762–1771.
[48] A. Lohani, G. Singh, S.S. Bhattacharya, A. Verma, Interpenetrating polymer networks as innovative drug delivery systems, J. Drug Deliv. 2014 (2014) 583612.
[49] X. Liu, H. Guo, L. Zha, Study of pH/temperature dual stimuli-responsive nanogels with interpenetrating polymer network structure, Polym. Int. 61 (7) (2012) 1144–1150.
[50] E. Zhang, J. Laufer, P. Beard, Backward-mode multiwavelength photoacoustic scanner using a planar Fabry-Perot polymer film ultrasound sensor for high-resolution three-dimensional imaging of biological tissues, Appl. Opt. 47 (4) (2008) 561–577.
[51] J. Buchmann, J. Guggenheim, E. Zhang, C. Scharfenorth, B. Spannekrebs, C. Villringer, J. Laufer, Characterization and modeling of Fabry–Perot ultrasound sensors with hard dielectric mirrors for photoacoustic imaging, Appl. Opt. 56 (17) (2017) 5039–5046.
[52] B.E. Treeby, B.T. Cox, k-Wave: MATLAB Toolbox for the Simulation and Reconstruction of Photoacoustic Wave Fields, SPIE, 2010.
[53] B.E. Treeby, J. Jaros, B.T. Cox, Advanced Photoacoustic Image Reconstruction Using the k-Wave Toolbox, SPIE, 2016.
[54] M. Molina, S. Wedepohl, E. Miceli, M. Calderón, Overcoming drug resistance with on-demand charged thermoresponsive dendritic nanogels, Nanomedicine 12 (2) (2017) 117–129.
[55] E. Lopez-Cabarcos, D. Mecerreyes, B. Sierra-Martin, M.S. Romero-Cano, P. Strunz, A. Fernandez-Barbero, Structural study of poly (N-isopropylacrylamide) microgels interpenetrated with polypyrrole, Phys. Chem. Chem. Phys. 6 (7) (2004) 1396–1400.
[56] D.E. Owens, N.A. Peppas, Opsonization, biodistribution, and pharmacokinetics of polymeric nanoparticles, Int. J. Pharm. 307 (1) (2006) 93–102.
[57] S.C. Nguyen, Q. Zhang, K. Manthiram, X. Ye, J.P. Lomont, C.B. Harris, H. Weller, A.P. Alivisatos, Study of heat transfer dynamics from gold nanorods to the environment via time-resolved infrared spectroscopy, ACS Nano 10 (2) (2016) 2144–2151.
[58] A. Rafiei Miandashti, L. Khosravi Khorashad, A.O. Govorov, M.E. Kordesch, H.H. Richardson, Time-resolved temperature-jump measurements and theoretical simulations of nanoscale heat transfer using NaYF4:Yb3+:Er3+ upconverting nanoparticles, J. Phys. Chem. C 123 (6) (2019) 3770–3780.
[59] J. Dybal, M. Trchová, P. Schmidt, The role of water in structural changes of poly(N-isopropylacrylamide) and poly(N-isopropylmethacrylamide) studied by FTIR, Raman spectroscopy and quantum chemical calculations, Vibrat. Spectr. 51 (1) (2009) 44–51.
[60] M.J. Ernsting, M. Murakami, A. Roy, S.-D. Li, Factors controlling the pharmacokinetics, biodistribution and intratumoral penetration of nanoparticles, J. Control. Release 172 (3) (2013) 782–794.
[61] J.P.M. Almeida, A.L. Chen, A. Foster, R. Drezek, In vivo biodistribution of nanoparticles, Nanomedicine 6 (5) (2011) 815–835.
[62] K. Raza, P. Kumar, N. Kumar, R. Malik, 9 - Pharmacokinetics and biodistribution of the nanoparticles, in: S. Nimesh, R. Chandra, N. Gupta (Eds.), Advances in Nanomedicine for the Delivery of Therapeutic Nucleic Acids, Woodhead Publishing, 2017, pp. 165–186.
[63] M. Neagu, Z. Piperigkou, K. Karamanou, A.B. Engin, A.O. Docea, C. Constantin, C. Negrei, D. Nikitovic, A. Tsatsakis, Protein bio-corona: critical issue in immune nanotoxicology, Arch. Toxicol. 91 (3) (2017) 1031–1048.
[64] H. Gao, J. Xiong, T. Cheng, J. Liu, L. Chu, J. Liu, R. Ma, L. Shi, In vivo biodistribution of mixed shell micelles with tunable hydrophilic/hydrophobic surface, Biomacromolecules 14 (2) (2013) 460–467.
[65] S.-D. Li, L. Huang, Pharmacokinetics and biodistribution of nanoparticles, Mol. Pharm. 5 (4) (2008) 496–504.
[66] S. Mitragotri, J. Lahann, Physical approaches to biomaterial design, Nat. Mater. 8 (2009) 15.